

MATHEMATICAL APPROACH TO REDESIGN OF A PARALLEL KINEMATIC CNC MACHINE

Kinematics, stiffness and singularity analysis

GEIR MAGNE EILERTSEN OLSEN

SUPERVISOR
Jan Christian Bjerke Strandene

Acknowledgements

Though this report only has one author, it has not been a work done alone. Here are a few names of people who were especially willing to give of their time and energy. It is an incomplete list because for a complete one it would be easier to just list the people who didn't help me at one time or another.

Firstly I want to thank the company representative who helped me with my thesis Jan Fredrik Røsjordet. His e-mail game is on point; Always a combination of extremely clear and concise communication combined with a very rapid response time. It was a great help during the thesis to have such a competent individual only an e-mail away. Also I would like to thank Professor Ali Mohammad Poursina, who is very generous with the giving of his time for questions unannounced. His student interactions also has a very good mix of guiding a student towards an answer while not giving the answer outright. Also worthy of note is fellow students Tarjei Skotterud and Martin Mæland. They were always busy but never too busy to discuss my problems. Their time was greatly appreciated.

Lastly a special acknowledgement goes to the supervisor Jan Christian Strandene, who was chosen by the administration due to lack of manpower and was multiple times during this thesis placed way out of his academic depths. He did not always provide clarity to my questions, but gosh darn it he tried his utmost and that alone deserves a lot of credit.

Abstract

This paper has created a basis for further development of the Hokarob Parallel Kinematic Machine (PKM) CNC machine. The machine currently has the ability to translate the head in three dimensions. The paper has focused on potential joint combinations to achieve two rotational degrees of freedom for the head of the machine. The solution has attempted to maintain the original work space, modularity and stiffness to as large a degree as possible while avoiding singularities. The paper has focused on developing the methods that can be applied alone or in combinations in this redesign process, rather than trying to find a viable solution to the entire problem. The methods have been implemented in Matlab code, but the results have also all been validated using either Simscape multibody simulations or Solidworks.

The paper starts off with a study of PKMs currently developed to draw inspiration from as well as a quick overview of math and geometry used in the report. The report then proposes several possible design changes that can be made, and the kinematic equations to solve these systems. Further a chapter is devoted to analyse what work space can at most be possible from the joint combinations suggested, both without and with taking into account the linkages of the PKM crashing into each other. A chapter then presents a simplified method to calculate stiffness of the PKM based only on the position of the linkages, and applies this to the different joint combinations while comparing results with the original system. Another chapter then suggests a quick method of comparing the different joint combinations to the original system for the purpose of systematizing the redesign process.

A chapter then combines all the information gathered and then uses it to create the best possible combination of joints to achieve the two new rotational degrees of freedom. A final section entails overall discussion and conclusion of the work, as well as suggesting a possible solution to the problem at hand using the methods developed in the paper. The solution suggested is in all likelihood not the best possible solution, but is a direction of future development that the author of this paper has confidence will eventually achieve its purpose very well. The section ends with a proposal for further developmental directions as well as a summary conclusion.

Contents

Acknowledgements	i
Abstract	ii
List of Figures	xiii
List of Tables	xv
1 Introduction	1
1.1 Introduction to parallel machines	1
1.2 Thesis requirements	2
1.3 Chapter structure	3
2 Theory	4
2.1 Examples of PKMs	4
2.1.1 The Stewart Platform	4
2.1.2 The Delta Picker	4
2.1.3 The Orthoglide	5
2.1.4 The Tricept T9000	6
2.1.5 The Ecospeed	8
2.1.6 SigmaTau	8
2.1.7 P-series CNC Centre	8
2.1.8 Linapod PKM	9
2.1.9 Arrow Project	10
2.1.10 Hybrid mechanism for computer assisted bone reduction surgery	10
2.2 Machining basics	11
2.3 Singularities	12
2.4 Newton-Raphson's method for higher dimensions	13
2.5 Gaussian rotation matrices	14
2.5.1 The cosine rule	15
3 Concepts	16
3.1 System as is	16
3.2 Wrist joint	18
3.3 Extending links	19
3.4 Rotational sleds	20
3.5 Revolute frame	21
3.6 Revolute gantry	22
3.7 Delta light concept	23
3.8 Double sled concept	24
4 Mobility testing	26
4.1 Testing scheme	26
4.2 Extending links	29
4.2.1 Pure kinematic potential in all directions	29

4.2.2	Kinematic potential while taking linkage geometry into account in X-rotation	30
4.3	Delta Light	31
4.3.1	Pure kinematic potential in all directions	31
4.3.2	Kinematic potential while taking linkage geometry into account in X-rotation	32
4.4	Rotational sleds	33
4.4.1	Pure kinematic potential in all directions	33
4.4.2	Kinematic potential while taking linkage geometry into account in X-rotation	34
4.5	Double Sled	35
4.5.1	Pure kinematic potential in all directions	35
4.5.2	Kinematic potential while taking linkage geometry into account in X-rotation	36
4.6	Discussion	36
5	Stiffness and Singularity Testing	37
5.1	Simplified stiffness calculation method	37
5.2	System as is	40
5.3	Extending links	41
5.3.1	45 degrees	41
5.3.2	90 degrees	42
5.4	Rotation sleds	43
5.4.1	45 degrees	43
5.4.2	90 degrees	44
5.5	Delta light	45
5.5.1	30 degrees	45
5.5.2	50 degrees	46
5.6	Double sled	47
5.6.1	45 degrees	47
5.6.2	90 degrees	48
6	Comparison to Original System	49
6.1	Extending links	50
6.2	Delta light	51
6.3	Rotational sled	52
6.4	Double sled	53
7	Final Result	54
7.1	Choosing concept	54
7.2	Removing the singularities	55
7.3	Final implementation	59
8	Discussion	61
8.1	Problems with the mobility graphs	61
8.2	Assumptions during stiffness calculations	61
8.3	Problems with the final Implementation	62
8.4	Future work	62
9	Conclusions	64
A	Stiffness graphs for extending links concept	65
A.1	10 Degrees	66
A.2	20 Degrees	67
A.3	30 Degrees	68
A.4	40 Degrees	69
A.5	50 Degrees	70
A.6	60 Degrees	71
A.7	70 Degrees	72

A.8	80 Degrees	73
A.9	90 Degrees	74
B	Stiffness graphs for rotational sleds concept	75
B.1	10 Degrees	75
B.2	20 Degrees	76
B.3	30 Degrees	77
B.4	40 Degrees	78
B.5	50 Degrees	79
B.6	60 Degrees	80
B.7	70 Degrees	81
B.8	80 Degrees	82
B.9	90 Degrees	83
C	Stiffness graphs for delta light concept	84
C.1	10 Degrees	84
C.2	20 Degrees	85
C.3	30 Degrees	86
C.4	40 Degrees	87
C.5	50 Degrees	88
C.6	60 Degrees	89
D	Stiffness graphs for double sled concept	90
D.1	10 Degrees	91
D.2	20 Degrees	92
D.3	30 Degrees	93
D.4	40 Degrees	94
D.5	50 Degrees	95
D.6	60 Degrees	96
D.7	70 Degrees	97
D.8	80 Degrees	98
D.9	90 Degrees	99
E	Various code snippets used in this report in Matlab code	100
E.1	Stiffness calculation script for system as is	100
E.2	Various functions used in the scripts	102
E.3	Script for a Newton-Raphson solver calculating new global positions for rotation around XZ-axis for head given a X-rotation of head	103
E.4	Newton-Raphson solver for finding one of the joint positions of the rotational sled	104
E.5	Script algebraically calculating both joint positions of the delta light concept	106
E.6	An example of a compare script for double sled concept	107
Bibliography		111

List of Figures

1.1	Standard 6-DOF robotic arm with gripper attachment [3]	1
1.2	The robot created by Hokarob, Source: Jan Fredrik Røsjordet	2
1.3	The robot created by Hokarob with see-through frame	2
2.1	Figure showing a small desktop Stewart platform with all neccessary components [4]	4
2.2	The ABB IRB 390 seen from above [15]	5
2.3	The ABB IRB 390 seen from below [15]	5
2.4	Drawing showing mechanical system in the Orthoglide 3-DOF [11]	6
2.5	Sketch of the workspace for the Orthoglide 3-DOF [11]	6
2.6	Orthoglide 5-DOF real world render [14]	6
2.7	Overview of the Orthoglide 2-DOF Wrist Joint Mechanism [14]	6
2.8	Picture of Tricept T9000 [12]	7
2.9	Graph showing T9000 working area with head at 45° [12]	7
2.10	Tricept T9000 wrist joint with side cover removed [16]	7
2.11	Ecospeed F 2035 machining centre [6]	8
2.12	Ecospeed PKM driver [5]	8
2.13	SigmaTau with a conventional wrist joint attached [7]	9
2.14	SigmaTau product demonstration video [1]	9
2.15	Consept picture of the Metrom P700 [2]	9
2.16	Head of the P700 [2]	9
2.17	CAD drawing and diagram of the Linapod [13]	10
2.18	Prototype pick and place robot called IRSB-bot	10
2.19	Prototype milling machine called ARROW-LIRMM	10
2.20	Sketch showing the joint distribution of the hybrid mechanism [9]	11
2.21	The hybrid mechanism in action [9]	11
2.22	Diagram showing cube sides numbering scheme	12
2.23	Situation showing flaw inherent in the design	12
2.24	Diagram showing a singularity having occurred in 2D	12
2.25	Newtons method in action, showing how the guess becomes incrementally closer to zero [10]	13
2.26	Input data for Gaussian rotation matrix	14
2.27	Position calculated using two different sets of Bryant angles	14
2.28	Diagram for explaining the cosine rule	15
3.1	Partial diagram of the current mechanism configuration	16
3.2	Joint mechanism as it currently exists	16
3.3	Image showing coordinate system of the machine	17
3.4	Diagram showing workspace of the current machine	17
3.5	Image showing naming scheme for the linkages and Tool Centre Point (TCP)	18
3.6	Figure showing vector calculation model for system as is with TCP in origin	18
3.7	Image showing head with relevant points	18
3.8	Concept model of a wrist joint solution	19
3.9	Partial diagram of the extending links concept	19
3.10	Partial diagram of the rotational sled concept	20
3.11	Diagram showing the four bar linkage of the rotational sled	20

3.12	Rotational sled positional diagram	20
3.13	Partial diagram of the rotational frame concept	22
3.14	Partial diagram of the rotational frame concept	22
3.15	Partial diagram showing the delta light concept	23
3.16	Delta light kinematic diagram	23
3.17	Partial diagram showing the double sled concept	25
4.1	Negative Y-rotation maximum travel	27
4.2	Diagram showing how impact is calculated in negative Y-direction	27
4.3	Maximum kinematic potential for extending links concept in positive Y-direction . .	29
4.4	Maximum kinematic potential for extending links concept in negative Y-direction .	29
4.5	Maximum kinematic potential for extending links concept in positive X-direction .	29
4.6	Maximum kinematic potential for extending links concept in negative X-direction .	29
4.7	Max possible rotation positive X while taking into account impact of linkages . .	30
4.8	Max possible rotation neg X while taking into account impact of linkages	30
4.9	Maximum kinematic potential for delta light concept in positive Y-direction	31
4.10	Maximum kinematic potential for delta light concept in negative Y-direction	31
4.11	Maximum kinematic potential for delta light concept in positive X-direction . . .	31
4.12	Maximum kinematic potential for delta light concept in negative X-direction	31
4.13	Max possible rotation positive X while taking into account impact of linkages . .	32
4.14	Max possible rotation neg X while taking into account impact of linkages	32
4.15	Maximum kinematic potential for rotational sled concept in positive Y-direction . .	33
4.16	Maximum kinematic potential for rotational sled concept in negative Y-direction .	33
4.17	Maximum kinematic potential for rotational sled concept in positive X-direction .	33
4.18	Maximum kinematic potential for rotational sled concept in negative X-direction .	33
4.19	Max possible rotation positive X while taking into account impact of linkages . .	34
4.20	Max possible rotation neg X while taking into account impact of linkages	34
4.21	Maximum kinematic potential for double sled concept in positive Y-direction	35
4.22	Maximum kinematic potential for double sled concept in negative Y-direction	35
4.23	Maximum kinematic potential for double sled concept in positive X-direction . . .	35
4.24	Maximum kinematic potential for double sled concept in negative X-direction	35
4.25	Max possible rotation positive X while taking into account impact of linkages . .	36
4.26	Max possible rotation neg X while taking into account impact of linkages	36
5.1	Figure showing sectioning and equivalent stiffness of the linkage	37
5.2	Stiffness for system as is for load in X-direction	40
5.3	Stiffness for system as is for load in Y-direction	40
5.4	Stiffness for system as is for load in Z-direction	40
5.5	System as is condition number for matrix inversion	40
5.6	Stiffness for extending links at 45 degrees for load in X-direction	41
5.7	Stiffness for extending links at 45 degrees for load in Y-direction	41
5.8	Stiffness for extending links in 45 degrees for load in Z-direction	41
5.9	Extending links condition number for matrix inversion for extending links concept at 45 degrees head angle	41
5.10	Stiffness for extending links for load in X-direction for extending links concept at 90 degrees head angle	42
5.11	Stiffness for extending links for load in Y-direction for extending links concept at 90 degrees head angle	42
5.12	Stiffness for extending links for load in Z-direction for extending links concept at 90 degrees head angle	42
5.13	Extending links condition number for matrix inversion for extending links concept at 90 degrees head angle	42
5.14	Stiffness for rotational sled concept for load in X-direction at 45° head angle	43
5.15	Stiffness for rotational sled concept for load in Y-direction at 45° head angle	43
5.16	Stiffness for rotational sled concept for load in Z-direction at 45° head angle	43

5.17	Rotational concept condition number for matrix inversion at 45° head angle	43
5.18	Stiffness for rotational sled concept for load in X-direction at 90° head angle	44
5.19	Stiffness for rotational sled concept for load in Y-direction at 90° head angle	44
5.20	Stiffness for rotational sled concept for load in Z-direction at 90° head angle	44
5.21	Rotational sled concept condition number for matrix inversion at 90° head angle . .	44
5.22	Stiffness for delta light concept for load in X-direction at 30° head angle	45
5.23	Stiffness for delta light concept for load in Y-direction at 30° head angle	45
5.24	Stiffness for delta light concept for load in Z-direction at 30° head angle	45
5.25	Delta light concept condition number for matrix inversion at 30° head angle	45
5.26	Stiffness for delta light concept for load in X-direction at 50° head angle	46
5.27	Stiffness for delta light concept for load in Y-direction at 50° head angle	46
5.28	Stiffness for delta light concept for load in Z-direction at 50° head angle	46
5.29	Delta light concept condition number for matrix inversion at 50° head angle	46
5.30	Stiffness for double sled for load in X-direction at 45° head angle	47
5.31	Stiffness for double sled for load in Y-direction at 45° head angle	47
5.32	Stiffness for double sled for load in Z-direction at 45° head angle	47
5.33	Double sled condition number for matrix inversion at 45° head angle	47
5.34	Stiffness for double sled for load in X-direction at 90° head angle	48
5.35	Stiffness for double sled for load in Y-direction at 90° head angle	48
5.36	Stiffness for double sled for load in Z-direction at 90° head angle	48
5.37	Double sled condition number for matrix inversion at 90° head angle	48
6.1	Maximum rotational angle while maintaining stiffness in X-direction	50
6.2	Maximum rotational angle while maintaining stiffness in Y-direction	50
6.3	Maximum rotational angle while maintaining stiffness in Z-direction	50
6.4	Maximum rotational angle while maintaining stiffness in X-direction	51
6.5	Maximum rotational angle while maintaining stiffness in Y-direction	51
6.6	Maximum rotational angle while maintaining stiffness in Z-direction	51
6.7	Maximum rotational angle while maintaining stiffness in X-direction	52
6.8	Maximum rotational angle while maintaining stiffness in Y-direction	52
6.9	Maximum rotational angle while maintaining stiffness in Z-direction	52
6.10	Maximum rotational angle while maintaining stiffness in X-direction	53
6.11	Maximum rotational angle while maintaining stiffness in Y-direction	53
6.12	Maximum rotational angle while maintaining stiffness in Z-direction	53
7.1	Vector model showing singularity position	55
7.2	Vector model more clearly showing singularity position	55
7.3	The new stiffness in X-direction at 0°	56
7.4	The new stiffness in Y-direction at 0°	56
7.5	The new stiffness in Z-direction at 0°	56
7.6	The new condition number for matrix inversion at 0°	56
7.7	The new stiffness in X-direction at 45°	57
7.8	The new stiffness in Y-direction at 45°	57
7.9	The new stiffness in Z-direction at 45°	57
7.10	The new condition number for matrix inversion at 45°	57
7.11	The new stiffness in X-direction at 90°	58
7.12	The new stiffness in Y-direction at 90°	58
7.13	The new stiffness in Z-direction at 90°	58
7.14	The new condition number for matrix inversion at 90°	58
7.15	Maximum rotational angle while maintaining stiffness in X-direction for the new configuration	59
7.16	Maximum rotational angle while maintaining stiffness in Y-direction for the new configuration	59
7.17	Maximum rotational angle while maintaining stiffness in Z-direction for the new configuration	59

7.18	Potential solution using the double sled concept	60
7.19	The potential solution implemented to achieve five sided machining	60
8.1	Figure showing linkage link with force lines in blue for tension and red for compression	62
A.1	Stiffness for load in X-direction for extending links concept at 10° head angle	66
A.2	Stiffness for load in Y-direction for extending links concept at 10° head angle	66
A.3	Stiffness for load in Z-direction for extending links concept at 10° head angle	66
A.4	Condition number for matrix inversion for extending links concept at 10° head angle	66
A.5	Joint position at C2 for extending links concept at 10° head angle	66
A.6	Joint position at F2 for extending links concept at 10° head angle	66
A.7	Stiffness for load in X-direction for extending links concept at 20° head angle	67
A.8	Stiffness for load in Y-direction for extending links concept at 20° head angle	67
A.9	Stiffness for load in Z-direction for extending links concept at 20° head angle	67
A.10	Condition number for matrix inversion for extending links concept at 20° head angle	67
A.11	Joint position at C2 for extending links concept at 20° head angle	67
A.12	Joint position at F2 for extending links concept at 20° head angle	67
A.13	Stiffness for load in X-direction for extending links concept at 30° head angle	68
A.14	Stiffness for load in Y-direction for extending links concept at 30° head angle	68
A.15	Stiffness for load in Z-direction for extending links concept at 30° head angle	68
A.16	Condition number for matrix inversion for extending links concept at 30° head angle	68
A.17	Joint position at C2 for extending links concept at 30° head angle	68
A.18	Joint position at F2 for extending links concept at 30° head angle	68
A.19	Stiffness for load in X-direction for extending links concept at 40° head angle	69
A.20	Stiffness for load in Y-direction for extending links concept at 40° head angle	69
A.21	Stiffness for load in Z-direction for extending links concept at 40° head angle	69
A.22	Condition number for matrix inversion for extending links concept at 40° head angle	69
A.23	Joint position at C2 for extending links concept at 40° head angle	69
A.24	Joint position at F2 for extending links concept at 40° head angle	69
A.25	Stiffness for load in X-direction for extending links concept at 50° head angle	70
A.26	Stiffness for load in Y-direction for extending links concept at 50° head angle	70
A.27	Stiffness for load in Z-direction for extending links concept at 50° head angle	70
A.28	Condition number for matrix inversion for extending links concept at 50° head angle	70
A.29	Joint position at C2 for extending links concept at 50° head angle	70
A.30	Joint position at F2 for extending links concept at 50° head angle	70
A.31	Stiffness for load in X-direction for extending links concept at 60° head angle	71
A.32	Stiffness for load in Y-direction for extending links concept at 60° head angle	71
A.33	Stiffness for load in Z-direction for extending links concept at 60° head angle	71
A.34	Condition number for matrix inversion for extending links concept at 60° head angle	71
A.35	Joint position at C2 for extending links concept at 60° head angle	71
A.36	Joint position at F2 for extending links concept at 60° head angle	71
A.37	Stiffness for load in X-direction for extending links concept at 70° head angle	72
A.38	Stiffness for load in Y-direction for extending links concept at 70° head angle	72
A.39	Stiffness for load in Z-direction for extending links concept at 70° head angle	72
A.40	Condition number for matrix inversion for extending links concept at 70° head angle	72
A.41	Joint position at C2 for extending links concept at 70° head angle	72
A.42	Joint position at F2 for extending links concept at 70° head angle	72
A.43	Stiffness for load in X-direction for extending links concept at 80° head angle	73
A.44	Stiffness for load in Y-direction for extending links concept at 80° head angle	73
A.45	Stiffness for load in Z-direction for extending links concept at 80° head angle	73
A.46	Condition number for matrix inversion for extending links concept at 80° head angle	73
A.47	Joint position at C2 for extending links concept at 80° head angle	73
A.48	Joint position at F2 for extending links concept at 80° head angle	73
A.49	Stiffness for load in X-direction for extending links concept at 90° head angle	74
A.50	Stiffness for load in Y-direction for extending links concept at 90° head angle	74

C.14 Stiffness for delta light concept for load in Y-direction at 40° head angle	87
C.15 Stiffness for delta light concept for load in Z-direction at 40° head angle	87
C.16 Delta light concept condition number for matrix inversion at 40° head angle	87
C.17 Stiffness for delta light concept for load in X-direction at 50° head angle	88
C.18 Stiffness for delta light concept for load in Y-direction at 50° head angle	88
C.19 Stiffness for delta light concept for load in Z-direction at 50° head angle	88
C.20 Delta light concept condition number for matrix inversion at 50° head angle	88
C.21 Stiffness for delta light concept for load in X-direction at 60° head angle	89
C.22 Stiffness for delta light concept for load in Y-direction at 60° head angle	89
C.23 Stiffness for delta light concept for load in Z-direction at 60° head angle	89
C.24 Delta light concept condition number for matrix inversion at 60° head angle	89
D.1 Stiffness for double sled for load in X-direction at 10° head angle	91
D.2 Stiffness for double sled for load in Y-direction at 10° head angle	91
D.3 Stiffness for double sled for load in Z-direction at 10° head angle	91
D.4 Double sled condition number for matrix inversion at 10° head angle	91
D.5 Necessary sled separation at 10° head angle	91
D.6 Necessary sled separation at 10° head angle	91
D.7 Stiffness for double sled for load in X-direction at 20° head angle	92
D.8 Stiffness for double sled for load in Y-direction at 20° head angle	92
D.9 Stiffness for double sled for load in Z-direction at 20° head angle	92
D.10 Double sled condition number for matrix inversion at 20° head angle	92
D.11 Necessary sled separation at 20° head angle	92
D.12 Necessary sled separation at 20° head angle	92
D.13 Stiffness for double sled for load in X-direction at 30° head angle	93
D.14 Stiffness for double sled for load in Y-direction at 30° head angle	93
D.15 Stiffness for double sled for load in Z-direction at 30° head angle	93
D.16 Double sled condition number for matrix inversion at 30° head angle	93
D.17 Necessary sled separation at 30° head angle	93
D.18 Necessary sled separation at 30° head angle	93
D.19 Stiffness for double sled for load in X-direction at 40° head angle	94
D.20 Stiffness for double sled for load in Y-direction at 40° head angle	94
D.21 Stiffness for double sled for load in Z-direction at 40° head angle	94
D.22 Double sled condition number for matrix inversion at 40° head angle	94
D.23 Necessary sled separation at 40° head angle	94
D.24 Necessary sled separation at 40° head angle	94
D.25 Stiffness for double sled for load in X-direction at 50° head angle	95
D.26 Stiffness for double sled for load in Y-direction at 50° head angle	95
D.27 Stiffness for double sled for load in Z-direction at 50° head angle	95
D.28 Double sled condition number for matrix inversion at 50° head angle	95
D.29 Necessary sled separation at 50° head angle	95
D.30 Necessary sled separation at 50° head angle	95
D.31 Stiffness for double sled for load in X-direction at 60° head angle	96
D.32 Stiffness for double sled for load in Y-direction at 60° head angle	96
D.33 Stiffness for double sled for load in Z-direction at 60° head angle	96
D.34 Double sled condition number for matrix inversion at 60° head angle	96
D.35 Necessary sled separation at 60° head angle	96
D.36 Necessary sled separation at 60° head angle	96
D.37 Stiffness for double sled for load in X-direction at 70° head angle	97
D.38 Stiffness for double sled for load in Y-direction at 70° head angle	97
D.39 Stiffness for double sled for load in Z-direction at 70° head angle	97
D.40 Double sled condition number for matrix inversion at 70° head angle	97
D.41 Necessary sled separation at 70° head angle	97
D.42 Necessary sled separation at 70° head angle	97

D.43 Stiffness for double sled for load in X-direction at 80° head angle	98
D.44 Stiffness for double sled for load in Y-direction at 80° head angle	98
D.45 Stiffness for double sled for load in Z-direction at 80° head angle	98
D.46 Double sled condition number for matrix inversion at 80° head angle	98
D.47 Necessary sled separation at 80° head angle	98
D.48 Necessary sled separation at 80° head angle	98
D.49 Stiffness for double sled for load in X-direction at 90° head angle	99
D.50 Stiffness for double sled for load in Y-direction at 90° head angle	99
D.51 Stiffness for double sled for load in Z-direction at 90° head angle	99
D.52 Double sled condition number for matrix inversion at 90° head angle	99
D.53 Necessary sled separation at 90° head angle	99
D.54 Necessary sled separation at 90° head angle	99

List of Tables

5.1	Values and results used in stiffness calculations	38
7.1	changes to the system that remedies the singularity problem	55

Chapter 1

Introduction

This chapter will briefly introduce linear vs parallel machines, set the overall goals and requirements of the thesis and lastly have a brief overview of the chapter structure.

1.1 Introduction to parallel machines

A kinematic machine can be split into two different categories, linear and parallel. This distinction refers to how the motion is transmitted through the joints, while kinematic means the machines purpose is to move. In a linear kinematic machine the motion is transmitted linearly from one actuator to another. Think of the standard six degrees of freedom robot arm that is commonly used in for example car manufacture and complex assembly operations. An example of this kind of robot can be seen in Figure 1.1.

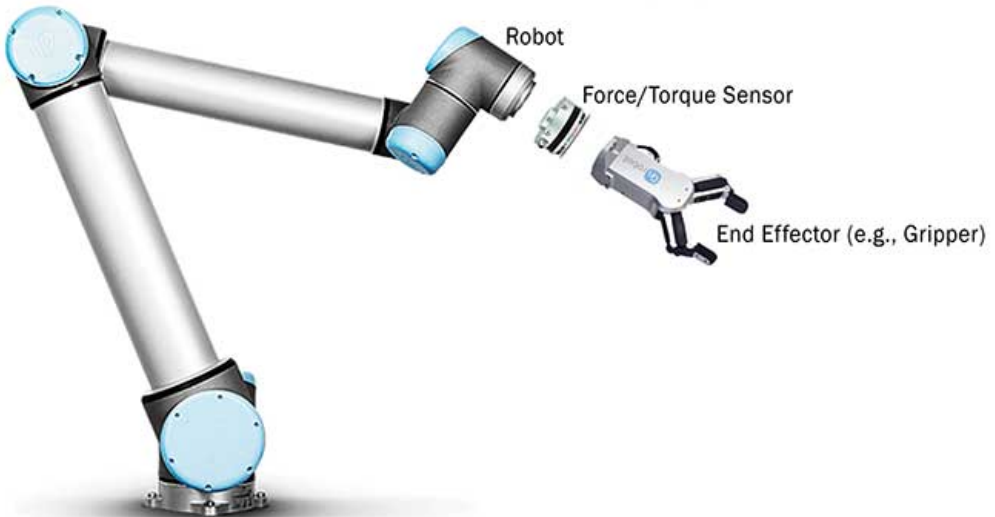


Figure 1.1: Standard 6-DOF robotic arm with gripper attachment [3]

A parallel kinematic machine (PKM) however has several kinematic chains that change the final position of the end effector, example seen in Figure 1.2. Here the end effector position will depend on several chains of joints working in parallel. This is obviously more complicated both mechanically and control systems wise. Also a parallel robot will tend to have significantly more singularities compared to a linear robot. A singularity is when the end effector of a system either loses or gains a degree of freedom. Designing parallel does however offer some interesting possibilities. PKMs does tend to be lighter than a linear robot while achieving significantly more stiffness of the end effector. PKMs also tend to be faster than a linear robot since more actuators can contribute to the end effector movement. The error of parallel robots tends to be smaller as well since the error is the average of the individual errors, rather than the linear robots that has the sum of the individual

errors as its final end effector error. These features makes the field of PKMs a highly desirable avenue of innovation and a hotly contested and quickly evolving marketplace full of innovation.

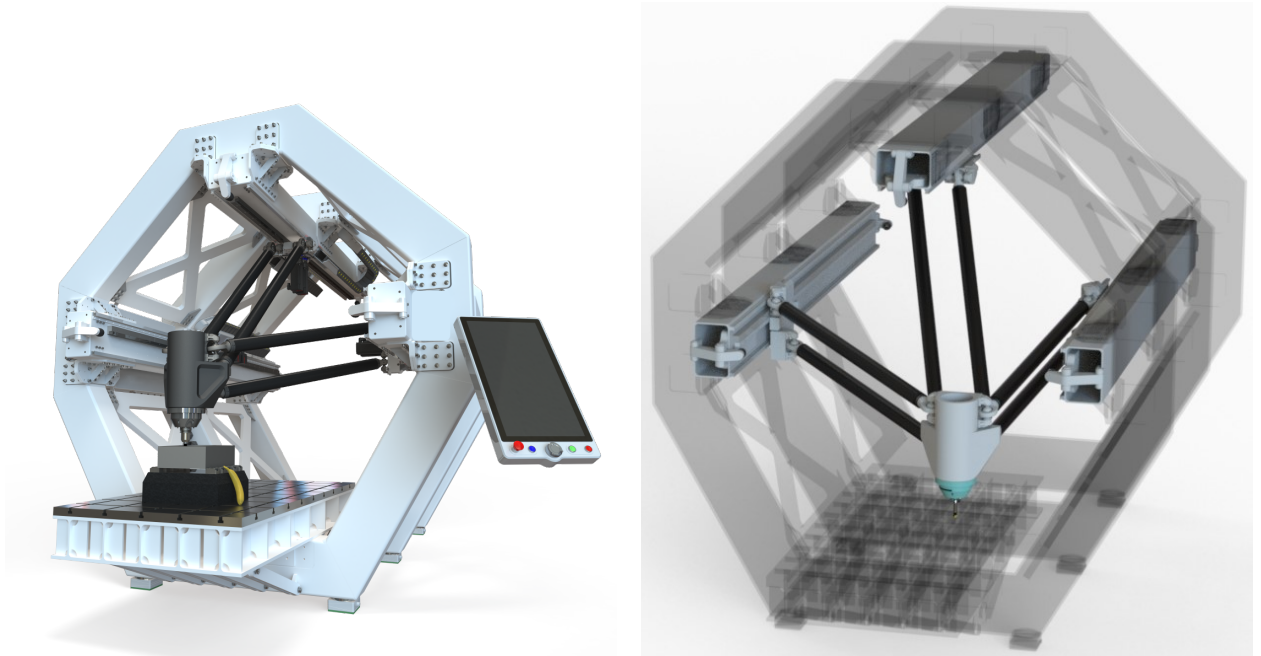


Figure 1.2: The robot created by Hokarob,
Source: Jan Fredrik Røsjordet

Figure 1.3: The robot created by Hokarob with
see-through frame

One of these innovators is Geir Hovland, who started the company Hokarob to bring his idea for a PKM CNC machine to life. It is currently under construction by Hokarob and can be seen in Figures 1.2 and 1.3. The machine has three degrees of Freedom (DOF), and a workspace of about 2x1x1 meters. The machine currently under construction will not be the final iteration however, as the plan is to be able to have a machine that can work on all sides of the work piece fully except the bottom side. This work is still early but this masters thesis will provide a groundwork for this future development. This thesis will do preliminary explorations into the possible directions the redesign can take. The thesis will not focus on creating a finished product, but rather suggesting a overall direction of the future development of the machine as well as collecting the tools required for this process.

1.2 Thesis requirements

The thesis has a few requirements. The end goal is to discover a development path that enables the head of the PKM to machine the work piece from all five sides, thus being able to rotate the tool point about two axes is essential. The thesis will focus on rotation of the tool point on the head. At least a rotation of $\pm 30^\circ$ has to be achieved, but a full $\pm 90^\circ$ is highly desirable. All development paths chosen needs to maintain the modularity of the system, meaning that the values calculated needs to be the same along the entire length of the machine. This is to aid quickly redesigning special configurations of the machine to suit specific markets. Lastly the computation method chosen needs to be compatible with all other. This might not be the optimal in all circumstances, but using the same method in all concepts will help clearly highlight the difference between the different development paths.

In all stages of the development a consideration to stiffness and singularities of the end effector will be kept in mind. Also in keeping with the design philosophy of parallel robots speed will be maximized for, so inertias will be a significant factor when weighting joints concepts. Since Hokarob

does not use the same tools internally (Matlab) that is used here, it is also attempted to only use functions that also exists in Python when creating the computation scripts. Lastly the equations and code presented in this report will forego dimensions of the actual system due to the competitiveness of the PKM market. Code with the dimensions removed can be found in its entirety in the [GitHub repo](#) with commit ID:'9182e67'.

1.3 Chapter structure

The thesis is structured as follows:

Chapter 2 : Theory	This chapter will detail a selection of the current market of PKMs, and briefly detail some math theory that will be used in this report
Chapter 3 : Concepts	This chapter will introduce the concepts that will be investigated in this report and show inverse kinematics of the ones deemed useful for further study
Chapter 4 : Mobility testing	This chapter will deploy the kinematics outlined in the previous chapter and find the maximum possible rotation both with and without checking for crashing of the linkages
Chapter 5 : Stiffness and Singularity Testing	This chapter will briefly outline a method for estimating stiffness of the system and find graphs for the remaining concepts in the direction chosen in the previous chapter
Chapter 6 : Comparison to Original System	This chapter will propose a way to categorize the stiffness data from the previous chapter
Chapter 7 : Final Result	This chapter will collate the results from previous chapters and suggest a potential implementation
Chapter 8 : Discussion	This chapter will discuss the results presented in the previous three chapters
Chapter 9 : Conclusion	This chapter will summarize the conclusions gained in the course of this project

Chapter 2

Theory

This chapter will serve as a limited introduction to the world of PKM design. It will begin with some market research showing which PKM solutions are currently available. Next is some terminology and PKM specific problems. The chapter ends with highlighting some math which will be useful later in the report.

2.1 Examples of PKMs

This chapter will discuss a limited number of examples of PKMs, and which joint combinations was chosen by its designers.

2.1.1 The Stewart Platform

The Stewart Platform is one of the two classical ways to create a 5-DOF PKM. It has been highly studied and is used in many different industries from wave simulation machines to flight simulators. It uses 6 actuated translational joints connected at both ends to 12 non-actuated Cardan joints (2-DOF rotational) joints.

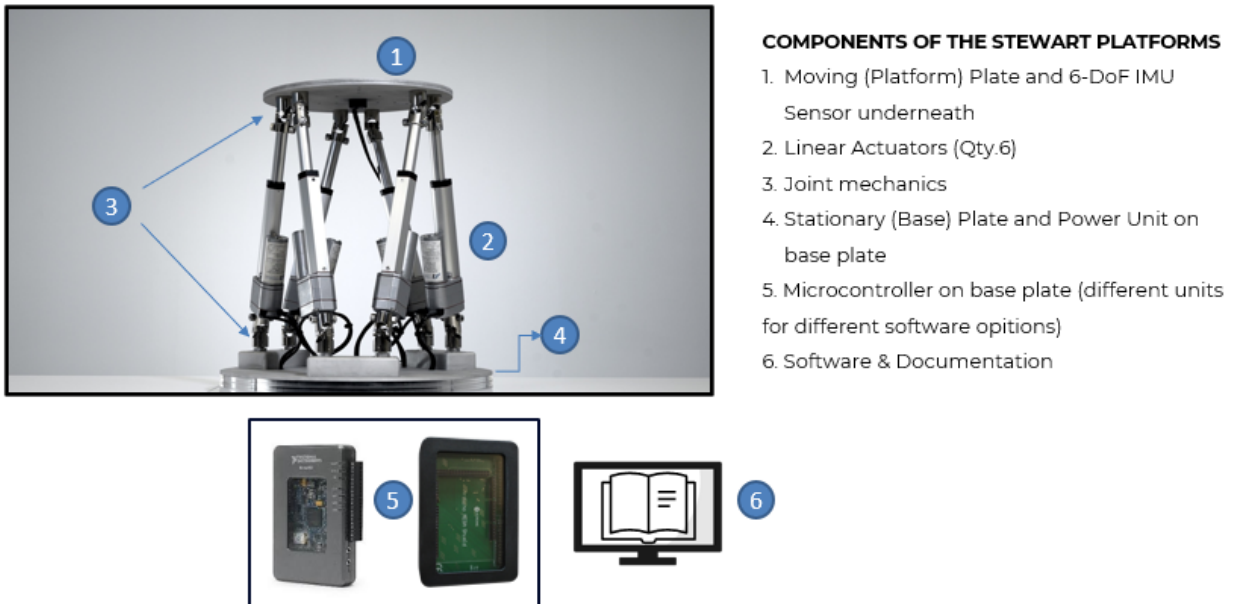


Figure 2.1: Figure showing a small desktop Stewart platform with all neccessary components [4]

2.1.2 The Delta Picker

The Delta picker design is the second classical way to make a 5-DOF PKM. The specific design mentioned here is the ABB IRB 390[15], but the design is implemented by many different companies

with very little changes to the joint configurations. The IRB 390 uses three actuated revolute joints and two actuated extending joint acting redundantly. This is connected to a common platform that can be moved in four directions, see Figure 2.2. A fifth movement axis can be attained using a wrist joint seen clearly in Figure 2.3.

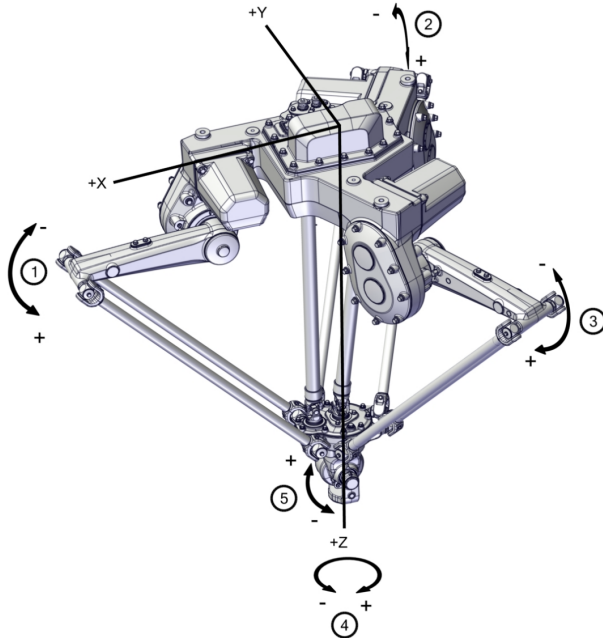


Figure 2.2: The ABB IRB 390 seen from above [15]

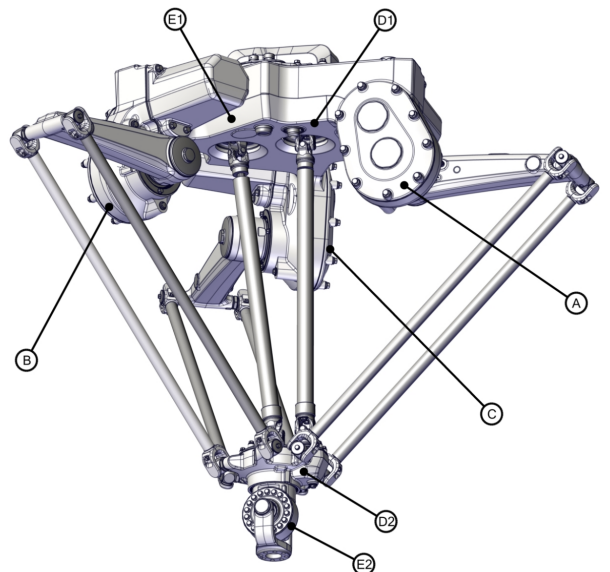


Figure 2.3: The ABB IRB 390 seen from below [15]

The delta design is known for high speed and control for small loads. This means it is used extensively in placement applications such as packaging and sorting. The design is unfortunately not very applicable for CNC applications since the 4-DOF 390 has a max payload of 15 kg, and the 5-DOF has a max payload of 10 kg.

2.1.3 The Orthoglide

The Orthoglide is a CNC machine developed by the Research Institute in Communications and Cybernetics of Nantes (IRCCyN), and comes in a 3-DOF and a 5-DOF variant. The 3-DOF can

only move in 3 translational coordinates. The PKM uses three actuated linear drivers and six non-actuated revolute joints to move the end effector. The three main axes of movement are perpendicular to each other which optimizes stress distribution between the members. Thus the 3-DOF boasts an impressive rigidity. Work space is however quite lacking and the foot print of the machine is very sparsely inhabited. A general sketch of the joints can be seen in figure 2.4, and the resulting workspace can be seen in Figure 2.5 [11].

The Orthoglide also comes in a 5-DOF variant, see Figure 2.6. The two added degrees of freedom comes from a wrist joint section that has been added to the Orthoglide 3-DOF PKM. The benefit of this decision is that the 3-DOF and the 5-DOF uses the same components, with the 5-DOF having the added wrist joint seen in Figure 2.7 [14]. The drawbacks is that the wrist joint is big and limits the rotational DOF quite a bit. It will also work counter to the benefits of the PKM design as the wrist joint is slow and heavy while the PKM is designed to be light and quick with a relatively big work space.

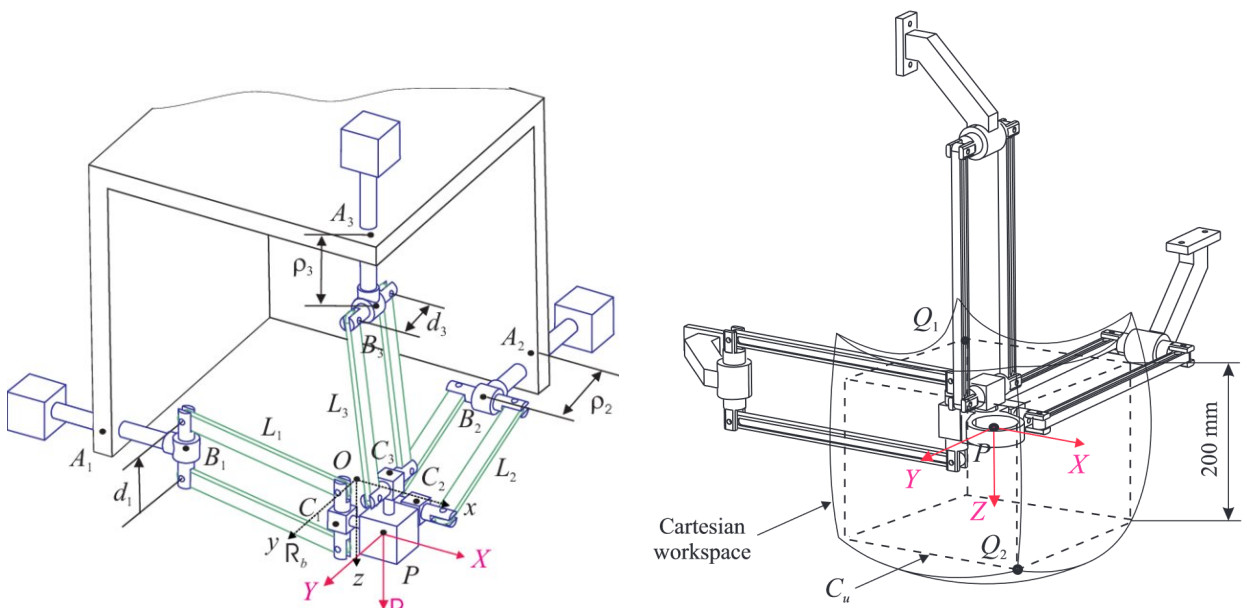


Figure 2.4: Drawing showing mechanical system in the Orthoglide 3-DOF [11]

Figure 2.5: Sketch of the workspace for the Orthoglide 3-DOF [11]

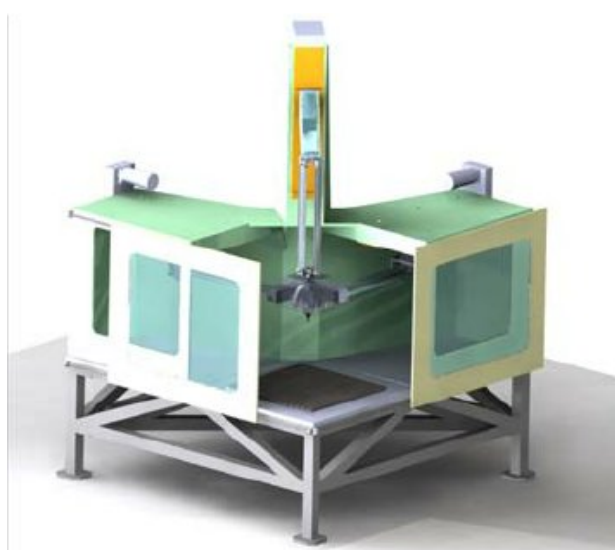


Figure 2.6: Orthoglide 5-DOF real world render [14]

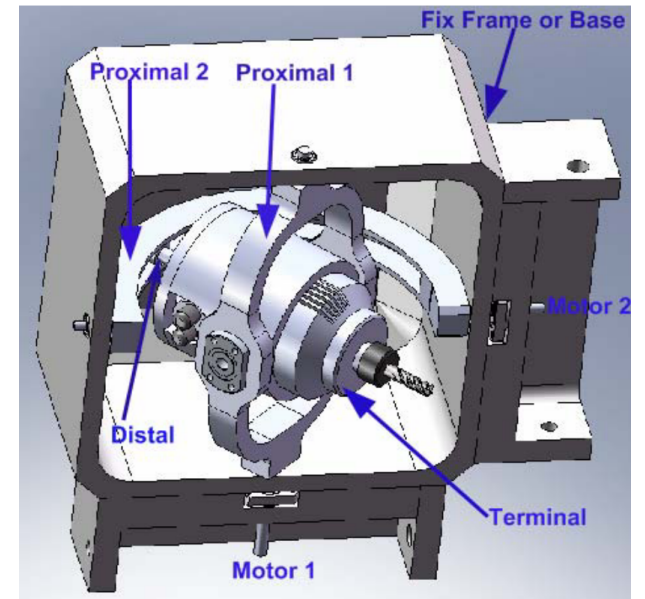


Figure 2.7: Overview of the Orthoglide 2-DOF Wrist Joint Mechanism [14]

2.1.4 The Tricept T9000

The Tricept CNC machine is a product range of PKM CNC machines produced by PKMTricept SL that has been popular for a long time. The T9000 has a 3-DOF PKM design composed of 3 actuated extending translational joints combined with 3 revolute joints and 3 spherical joints. The entire machine weighs 3400 kg, with the moving components totalling 900 kg. The machine is very stiff with horizontal stiffness of $120N/\mu m$ and vertical stiffness of $200N/\mu m$ [16]. The work area is impressively large at close to 3 meters horizontal and 1 meter vertical with ideal work piece positioning, as seen in Figure 2.9. The benefit of the Tricept is that it is sold as a single unit, see Figure 2.8. This means that it can easily be installed in many different orientations, with some manufacturers having multiple different models working on the same work piece at the same time.

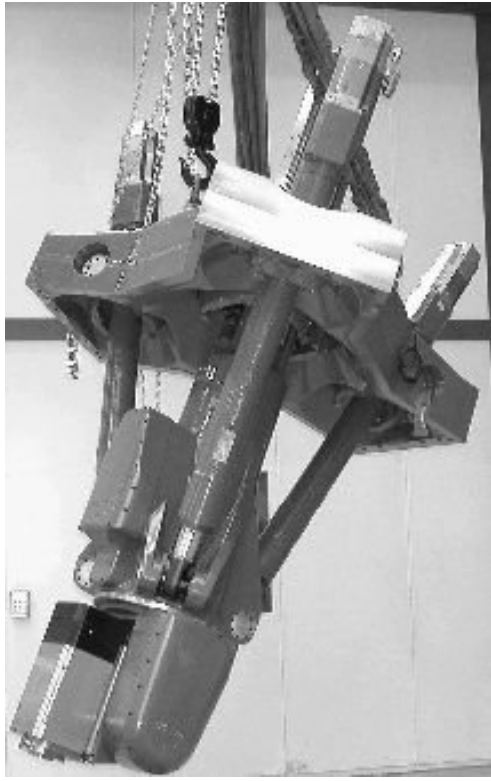


Figure 2.8: Picture of Tricept T9000 [12]

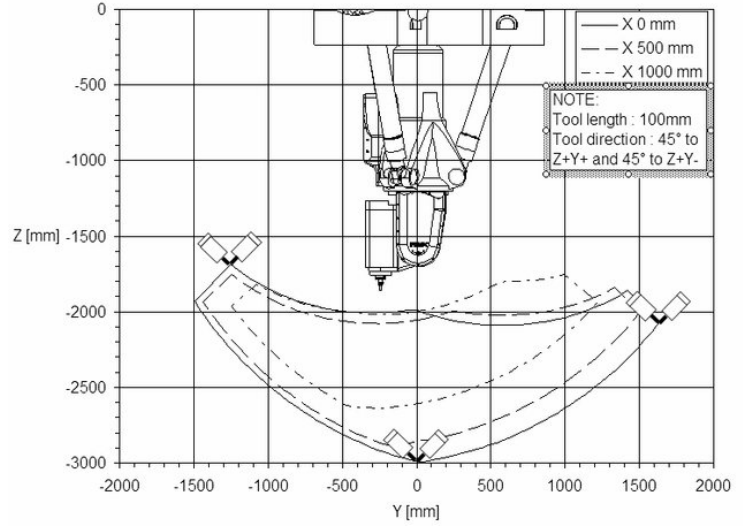


Figure 2.9: Graph showing T9000 working area with head at 45° [12]

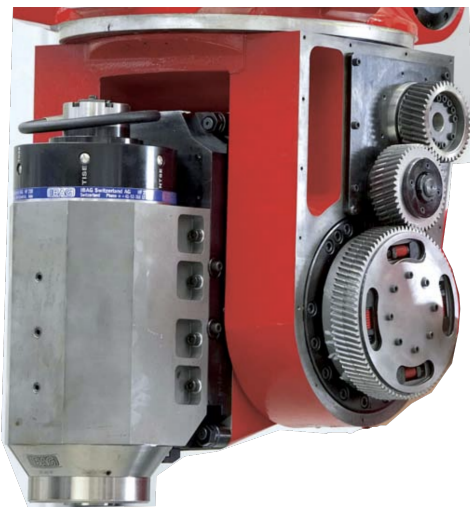


Figure 2.10: Tricept T9000 wrist joint with side cover removed [16]

The T9000 has a wrist joint at the main coupling point that permits the last two rotational degrees of freedom. The wrist can bend a full 360° in the main wrist joint and -5° to $+180^\circ$ in the secondary joint. The wrist joint can be more closely seen in Figure 2.10. The Tricept has been installed in hundreds of different applications, and is lauded for its robustness and reliability. It is however not a true 5-DOF PKM CNC machine since it only uses a 3-DOF PKM design with a 2-DOF wrist attachment at the end. It also uses an interesting and custom gearbox with a split gear that is spring loaded in both directions to eliminate backlash when changing direction. The wrist joint does however add a considerable amount of weight to the machine.

2.1.5 The Ecospeed

The ecospeed is a 5-DOF CNC centre produced by Starrag. It is a parallel kinematic 5-DOF machine that does not use a wrist joint as is common in the other machines mentioned, but is by far the largest PKM in this chapter. It features three actuated translational joints connected to the head using three non-actuated cylindrical joints, see Figure 2.12. The unit can also be moved perpendicular to the translational joints in both directions using actuated translational joints. Possible workspace 0.67 metres in axial direction and the different ecospeeds have different perpendicular translation. The head can rotate $\pm 45^\circ$ in both directions [5].

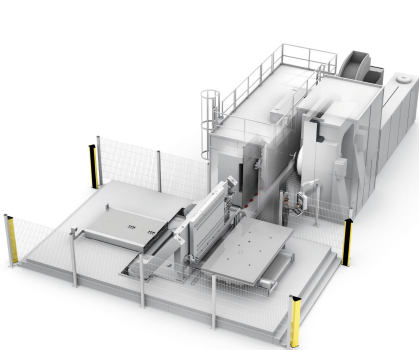


Figure 2.11: Ecospeed F 2035 machining centre [6]

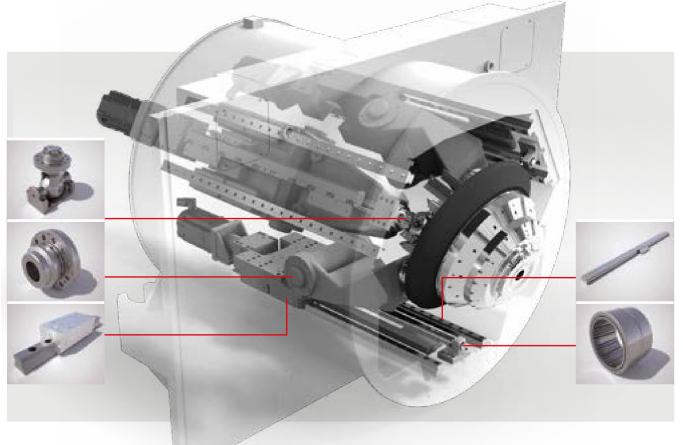


Figure 2.12: Ecospeed PKM driver [5]

The benefit of the ecospeed is that the toolpoint has an unobstructed possible rotation, i.e. that the rotation of the end effector is holonomic. This means that any rotary motion is possible, which is not the case when using a rotational wrist joint attachment. This makes the ecospeed quite popular within aviation industries since they have very complex geometry and size of the system is not as large a factor as it is in the production of more small scaled products.

2.1.6 SigmaTau

Cognibotics is a Swedish company started in 2013, but has recently diversified into the CNC market using its SigmaTau PKM. It is a 3-DOF PKM platform that has been optimized to be lightweight and rigid with a large head that can fit many different tools. This makes it an ideal platform for a diverse set of operations such as welding, machining or laser cutting. Figure 2.13 shows a screenshot from a product demonstration simulation with a machining head mounted on a standard wrist joint. Figure 2.14 shows a wrist joint actuated from the frame rather than the head using two linear actuators. This is a good way to reduce weight of the head and thus play to the strength of the PKM design.

Electrical linear actuators are generally more accurate than rotational actuators. Also a linear actuator will have a large part of the forces inline with the axis of motion, while a rotational driver will have shear forces no matter what position it is in. These considerations are part of the reason why most of the designs mentioned here use linear drivers. This design from Cognibotics takes advantage of the linear driver in a clever way both in the main translational joints and the wrist control scheme seen in Figure 2.14 .

2.1.7 P-series CNC Centre

The P700 from Metrom in Germany is a 5 axis CNC machining centre. It functions very similarly to a tricept design only it uses 5 actuated extending translational joints to move a CNC head. The



Figure 2.13: SigmaTau with a conventional wrist joint attached [7]



Figure 2.14: SigmaTau product demonstration video [1]

machining centre also comes equipped with a rotary and tilting table for complete 5 sided machining. The icosehedronic structure is chosen because it is the most stable and rigid geometric shape, and the final product can be seen in Figure 2.15.



Figure 2.15: Concept picture of the Metrom P700 [2]



Figure 2.16: Head of the P700 [2]

The designer of the P-series has decided to mount the machining head offset from the table axis, see Figure 2.16. A similar choice was made for the Sigma Tau, seen in Figure 2.14. This maximises the rotation in a single direction. If for example the possible rotation is $\pm 45^\circ$, then with the head mounted offset the possible rotation is instead $-0^\circ / + 90^\circ$ [2]. This combined with the rotation table will achieve complete 5 sided machining capabilities. This combination design is clever because PKMs generally have a large amount of interactions during rotation. This design decision means that only a single rotational direction needs to be functional to produce every possible rotation.

2.1.8 Linapod PKM

The Linapod is a design originating in the Institute for Control Engineering of Machine Tools and Manufacturing Units (ISW) in Stuttgart Germany. It uses six translational actuators to achieve six degrees of freedom at the head, seen in Figure 2.17.

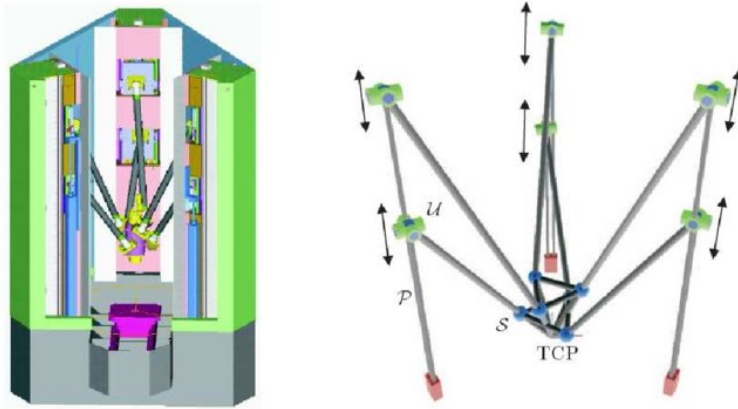


Figure 2.17: CAD drawing and diagram of the Linapod [13]

The paper is notable for its mathematical optimization approach to the design process, which yielded an extremely low weight but sturdy final product. Though the joint combination is nothing new, the optimization approach can be very useful when the design process comes to a more advanced stage.

2.1.9 Arrow Project

The Arrow project was created in October 2011 by The French Research Agency (ANR). Its purpose is to create robots that are both fast and accurate with a large possible workspace, since robotics generally can only achieve one of these parameters. The robots created would be geared towards industry, with an ideal acceleration of 20G with an accuracy of $20 \mu\text{m}$. Two Arrow prototypes will be quickly mentioned here. The first is a modified delta design with three actuated revolute joints and 8 non-actuated Cardan joints, seen in Figure 2.18. The second machine is a machine very much like the Linapod with six actuated translational joints and 12 non-actuated Cardan joints[8].

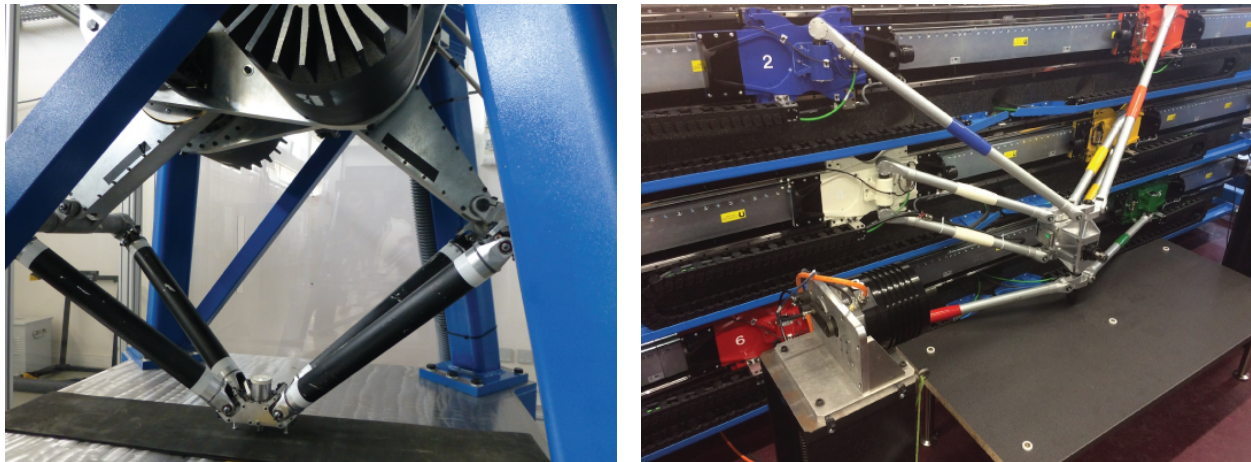


Figure 2.18: Prototype pick and place robot called IRSB-bot

Figure 2.19: Prototype milling machine called ARROW-LIRMM

This report will not spend an undue amount of time to summarize the whole Arrow project, but it is mentioned here as a rich source of different machines that attempts to accomplish roughly what this report has as overall future objective.

2.1.10 Hybrid mechanism for computer assisted bone reduction surgery

This unnamed mechanism is developed to fix breaks of large bones by aligning them exactly using computer software. It is created to replace the Ilizarov apparatus, which is a manually operated

stewart platform design in common use today. It operates by use of three actuated sliding translational joints and three actuated extending translational joints. The mechanism also requires six passive revolute joints and 3 passive translational joints as well as 3 passive ball socket joints. The design is shown in Figure 2.20, and shown in use in Figure 2.21.

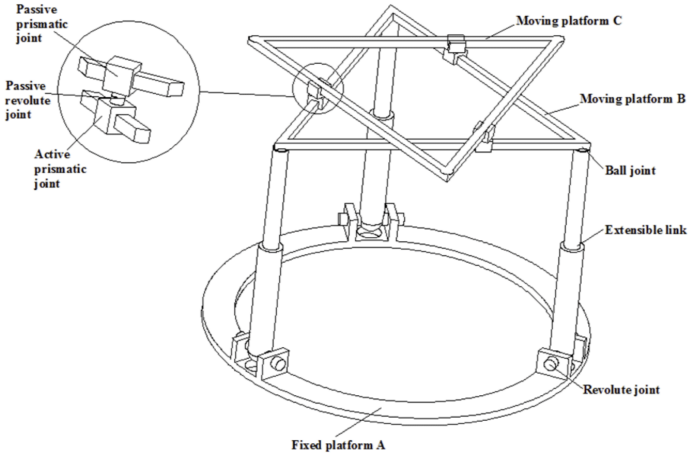


Figure 2.20: Sketch showing the joint distribution of the hybrid mechanism [9]

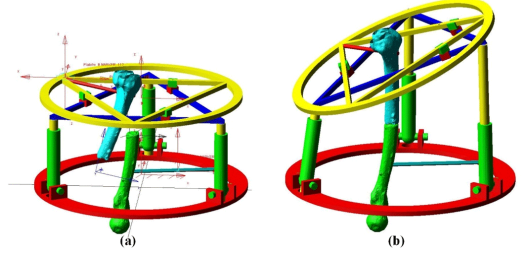


Figure 2.21: The hybrid mechanism in action [9]

The benefits of this mechanism is that all joints needed for the operation is kept close to the main frame of the device keeping weight where it is more easily supported. It also features a clever way to create rotational motion from linear actuators. The drawbacks are that the mechanism is very complex to implement and will have quite a few singularity positions where manual reset will be necessary. It will also have a very limited axial rotation radius. This paper will not elaborate further on these singular positions, but the paper [9] goes in to great detail about this specific problem.

2.2 Machining basics

This chapter will introduce what a CNC machine is, some specific terms used in this report as well as some problems specific to this CNC machine.

A CNC milling machine is a machine that can automatically drive a cutting tool, most often a drill bit, for the purpose of creating a geometric shape. Simple geometric shapes are generally created using more standard machines, so the niche CNC machines inhabit is the ability to create complex geometric shapes in few operations. Reducing the number of operations is important for optimizing the machining process because it lowers the amount of equipment needed to create a part as well as the amount of time. The time decreases further if the CNC machine has the ability to pivot more and thus remove more of the needed material in a single process. This is called full or partial n-sided machining, where n is the amount of sides that can be reached without manual intervention. The optimal work area of a CNC machine is to have conical angle of 90° of access to five sides of the work piece, see Figure 2.22. The sixth side is generally used to secure the piece to the work table and is very rarely machined on without rotating the work piece.

The particular machine in this report design has a flaw where the head needs the area behind it to be free for the arms to operate. This means that any rotation solution will most likely not encompass the shadow side of the work piece in the cube diagram Figure 2.22. See Figure 2.23 for an example showing this situation about to happen. This means that any concept chosen will most likely not be able to achieve five-sided machining without major re-design. Thus achieving five-sided machining with a single operation is not considered feasible going forward.

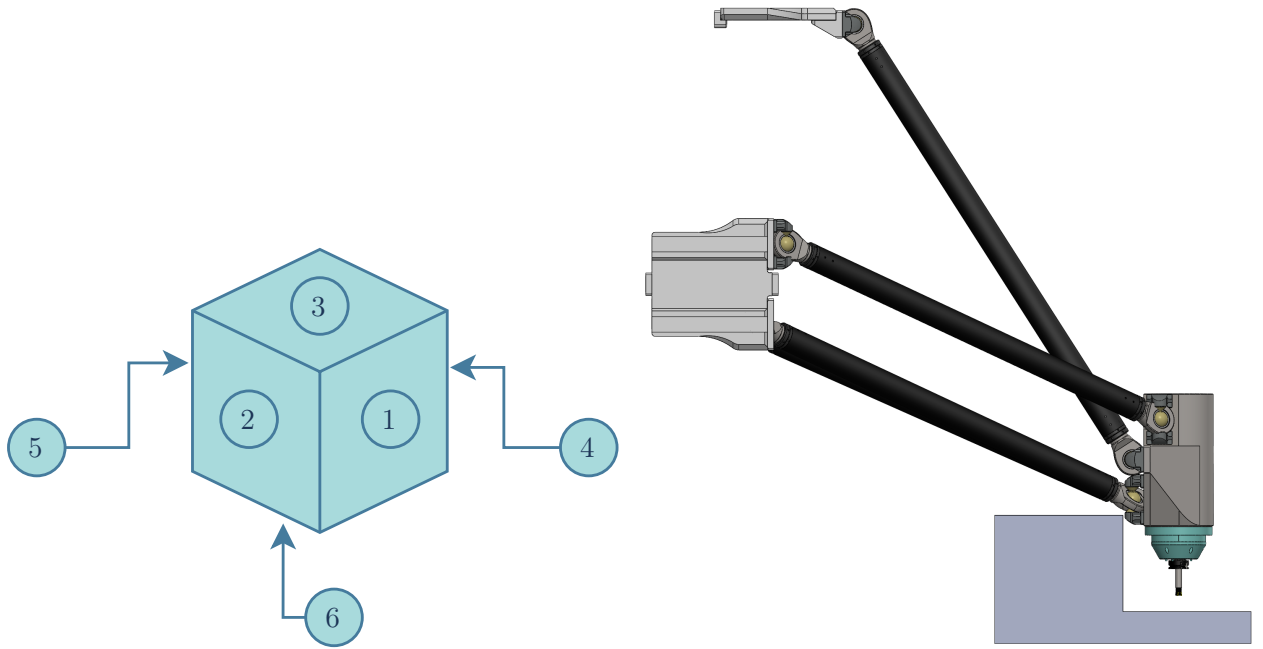


Figure 2.22: Diagram showing cube sides numbering scheme

Figure 2.23: Situation showing flaw inherent in the design

2.3 Singularities

This chapter will briefly describe what a singularity is. Singularities are when the bodies of a system has a geometry which causes the system of bodies to either lose a degree of freedom or gains a degree of freedom. In layman's terms: if a system moves to a certain position, then either it freezes or it drops unexpectedly. There is a problem with the latter in the system that this paper will investigate, so this chapter will quickly explain what happens when it drops and why this occurs. An example of a body which will be unconstrained in 2D, and therefore drop, can be seen in Figure 2.24.

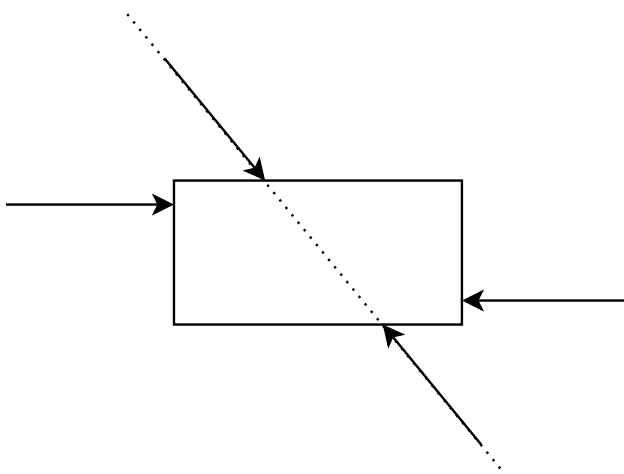


Figure 2.24: Diagram showing a singularity having occurred in 2D

A body in 3D space needs to be constrained in three movement directions and three rotational directions. If this force equilibrium is not in place then that will cause either an acceleration or a rotational acceleration. Constraining an object translationally requires only three forces in different directions, and will always be the case for this system. The constraint in rotation is however more prone to change within the workspace. Constraining the object rotationally requires three moments to be applied to it, therefore requiring six force pairs. If the line of action of one force hits another force, then the two forces become one force from a moment point of view. This means you lose one

of the force pairs, and the machine will rotate chaotically. Since the machine in question has six arms and thus six forces manipulating the head, then having two forces meet at the same place in space means that a singularity will occur. This singular distribution of forces has been schematically shown in 2D in Figure 2.24. In this figure the forces may cancel out but the moment the forces produces will never equal zero and thus the box will spin chaotically. This phenomena is decidedly not optimal when creating a CNC machine, and needs to be avoided on the final product.

2.4 Newton-Raphson's method for higher dimensions

This chapter will briefly explain what Newton's method is, and how it is implemented. Newton-Raphson's method is a numerical solving scheme to solve equations using an iterative approach that incrementally gets close to where the equation has a zero-point. Any equation solved using the Newton-Raphson method needs to be shifted so that zero is the value that is needed. The method has as inputs a point on the function and the derived of that point on the function. The method will then create a line from the point along the line of the derived of the function. This line is then followed to the zero line where a new point is input and a new derivative is taken into the schema. This method in action using several iterations (n), applied to a single equation (f) with a single variable (x), can be seen Figure 2.25 and in equation 2.1.

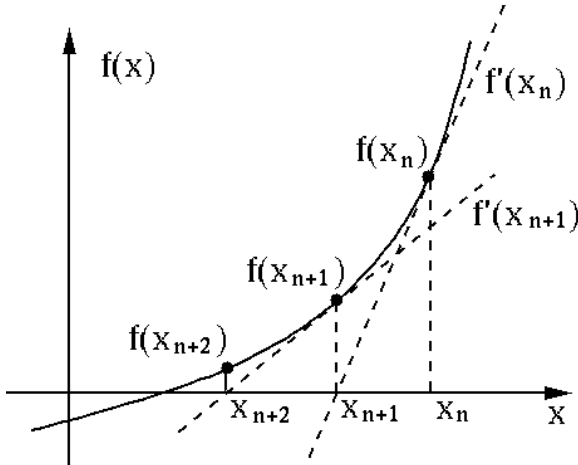


Figure 2.25: Newtons method in action, showing how the guess becomes incrementally closer to zero [10]

$$x_{n+1} = x_n - \frac{f(x_n)}{\frac{df}{dx_n}(x_n)} \quad (2.1)$$

The method can also be applied to any series of equations, so long as it is p equations with p unknowns between them. The schema works the same as in Figure 2.25, however the point and vector are both in p dimensions. This solver schema can be seen in equation 2.2, where bold characters represent matrices and vectors.

$$\begin{bmatrix} x_1^{(n+1)} \\ x_2^{(n+1)} \\ \vdots \\ x_p^{(n+1)} \end{bmatrix} = \begin{bmatrix} x_1^{(n)} \\ x_2^{(n)} \\ \vdots \\ x_p^{(n)} \end{bmatrix} - \begin{bmatrix} \frac{\delta f_1}{\delta x_1}(\mathbf{x}^{(n)}) & \dots & \dots & \frac{\delta f_1}{\delta x_p}(\mathbf{x}^{(n)}) \\ \frac{\delta f_2}{\delta x_1}(\mathbf{x}^{(n)}) & \ddots & \vdots & \vdots \\ \vdots & \vdots & \vdots & \vdots \\ \frac{\delta f_p}{\delta x_1}(\mathbf{x}^{(n)}) & \dots & \dots & \frac{\delta f_p}{\delta x_p}(\mathbf{x}^{(n)}) \end{bmatrix}^{-1} \cdot \begin{bmatrix} f_1(\mathbf{x}^{(n)}) \\ f_2(\mathbf{x}^{(n)}) \\ \vdots \\ f_p(\mathbf{x}^{(n)}) \end{bmatrix} \quad (2.2)$$

2.5 Gaussian rotation matrices

This chapter will briefly introduce the concept of Gaussian rotation matrices and how they are used. An implemented function of a Gaussian rotation matrix can be found in Appendix E.2. Gaussian rotation matrices allow you to calculate distances between points on a body where the body has rotated from its original orientation. The reason Gaussian matrices was chosen over quaternions is because the system starts at a point with a rotation of zero degrees, and will increment a single or multiple rotation directions until a break signal is achieved. It then resets to zero rotational angle and moves to another position and the same is done there. No further movements from the end position is needed and thus gimbal lock is not an issue. Therefore Gaussian matrices are sufficiently capable of finding a solution.

Gaussian rotation matrices will input a rotation around one or a series of axes, called in this report px, py and pz for the head or R for specific rotations. The individual matrices can be seen in equation 2.3. This matrix is then used to calculate the position of points in a local coordinate system of an object after object rotation, see equation 2.4 where marked position is original local coordinate. A is the Gaussian rotation matrix, with 1,2 and 3 being the chosen order of equation 2.3. It is important to note that the order of rotations is very important and a different order of rotations will impact the final end position of the point. This can be seen in Figure 2.27, where a point on the system is given a bidirectional rotation, Figure 2.26. The resulting position is calculated two ways, using $A_{xz} = A_x \cdot A_z$ and $A_{zx} = A_z \cdot A_x$. As can be seen the positions differ greatly and only one combination ended up calculating the position correctly.

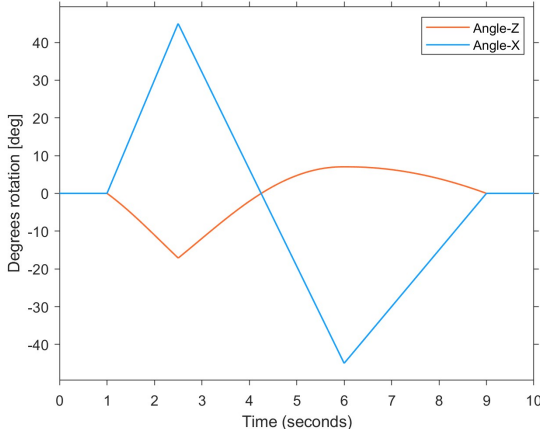


Figure 2.26: Input data for Gaussian rotation matrix

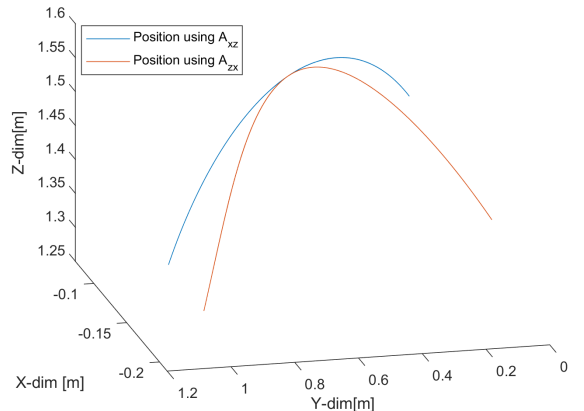


Figure 2.27: Position calculated using two different sets of Bryant angles

$$A_x = \begin{bmatrix} 1 & 0 & 0 \\ 0 & \cos(px) & -\sin(px) \\ 0 & \sin(px) & \cos(px) \end{bmatrix}, A_y = \begin{bmatrix} \cos(py) & 0 & \sin(py) \\ 0 & 1 & 0 \\ -\sin(py) & 0 & \cos(py) \end{bmatrix}, A_z = \begin{bmatrix} \cos(pz) & \sin(pz) & 0 \\ \sin(pz) & \cos(pz) & 0 \\ 0 & 0 & 1 \end{bmatrix} \quad (2.3)$$

$$pos_{current} = A \cdot pos', \text{ where } A = A_1 \cdot A_2 \cdot A_3 \quad (2.4)$$

2.5.1 The cosine rule

The cosine rule is taught to all engineers at a very early level, but it has a tendency to be forgotten. Therefore it is decided to be quickly shown here. Sine, cosine and tangent of angles is used in every area of engineering. They do however require that one of the three angles of the triangle is 90° . The cosine rule is an application that does not have this requirement.

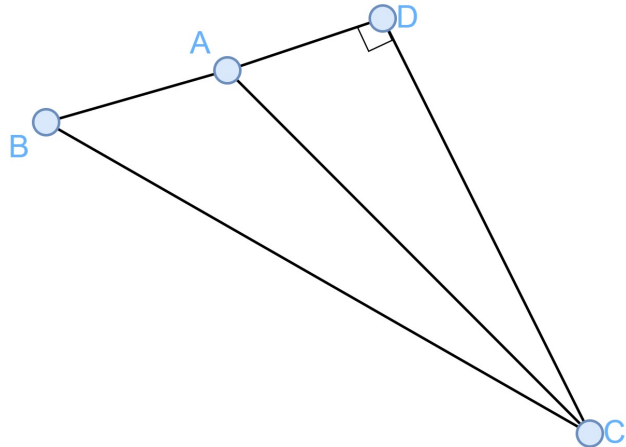


Figure 2.28: Diagram for explaining the cosine rule

The rule is seen in equation 2.5, with accompanying Figure 2.28. The important thing to know is that you are not solving for $\triangle ABC$, but rather for $\triangle DBC$. This is then used to calculate $\triangle ABC$, which means that $\triangle ABC$ does not have to have one square angle. The rule is generally used when three sides of the triangle is known and all of the angles are unknown. In this report the rule is used for its ability to

$$2 \cdot |CA| \cdot |CB| \cdot \cos(\angle CAB) = |CA|^2 + |AB|^2 - |CB|^2 \quad (2.5)$$

Chapter 3

Concepts

This chapter will introduce the different possibilities for increasing the DOF of the PKM. The different concepts will have a cursory examination and the concepts that warrant further examination will be brought forward to the next chapters. Kinematics of the concept will be determined if they warrant further examination.

The kinematic diagrams used in this report will rely on shapes to indicate joint position and degrees of freedom. The rectangular box represents a translational joint with a single degree of freedom along the long axis. The cylinder represents a revolute joint with a single degree of freedom around the axial direction. The sphere represents a spherical joint with three rotational degrees of freedom centered at the midpoint of the sphere. A diagram of one of the mechanisms as it exists today using this method of showing joints can be seen in Figure 3.1.

3.1 System as is

The joint system as it exists today is as following: Three sleds are connected to two ball socket joints each. These joints are connected to a constant length rod. These six rods are all connected to ball socket joints on the head. The only actuated joints are the three translational joints on the sleds. See Figure 3.2.

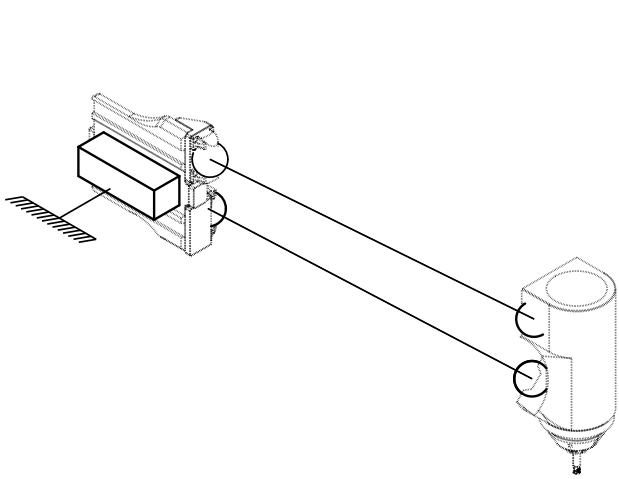


Figure 3.1: Partial diagram of the current mechanism configuration



Figure 3.2: Joint mechanism as it currently exists

The workspace of the current machine can be seen in yellow in Figures 3.3 and 3.4. The coordinate system is chosen to be located at the centre bottom edge of the workspace, and unless otherwise indicated, will be the coordinate system used throughout the report.

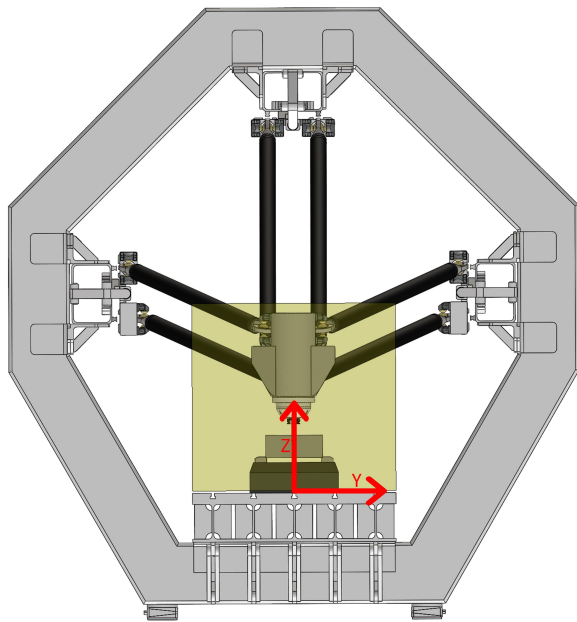


Figure 3.3: Image showing coordinate system of the machine

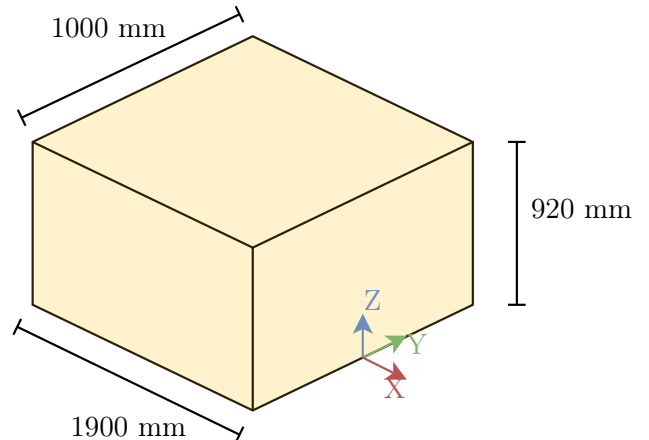


Figure 3.4: Diagram showing workspace of the current machine

The linkages are called Linkage A through Linkage F, see Figure 3.5. Linkages will be given the symbol L during calculations. The connecting points are called 1 if on the head and 2 if on the sled, see Figure 3.6 showing the vector model used further on in this report. Figure 3.7 shows the head from behind with the TCP in the origin. The linkages come in two different lengths, called L_{short} and L_{long} , with the long linkages connected to north sled and the short linkages connected to east and west sleds. Details of the linkages can be found in Table 5.1.

The kinematics of the system as it currently exists is quite simple. It is six constant distance constraints controlling six degrees of freedom on the head. The points on the sleds are rigidly connected to each other, and from an inverse kinematics view only one of these are needed to calculate the three x-coordinates the sled needs to occupy. This report calculates exclusively inverse kinematics, and thus the equations to be solved for the system as is can be seen in equation 3.1 and 3.2 with the two points being 85 mm apart in X-direction for east and west sled. North sled has equal X-coordinate of the two linkages. The equations can be solved in two different ways since $\pm\sqrt{\dots}$ gives two different solutions. The system as is works solely in left handed mode, thus the prefix of the square root is always negative.

$$\begin{aligned} L^2 &= (X_2 - X_1)^2 + (Y_2 - Y_1)^2 + (Z_2 - Z_1)^2 \\ &\downarrow \\ X_2 &= X_1 - \sqrt{L^2 - (Y_2 - Y_1)^2 - (Z_2 - Z_1)^2} \end{aligned} \tag{3.1}$$

$$X_{2,1} = X_{2,2} \pm 0.085 \tag{3.2}$$

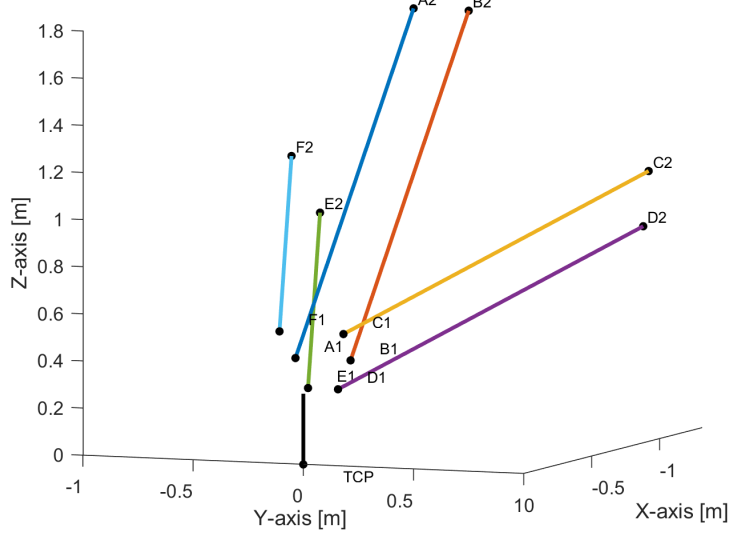
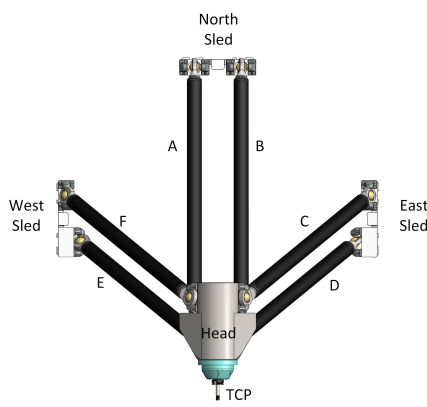


Figure 3.5: Image showing naming

scheme for the linkages and Tool Figure 3.6: Figure showing vector calculation model for system Centre Point (TCP) as is with TCP in origin

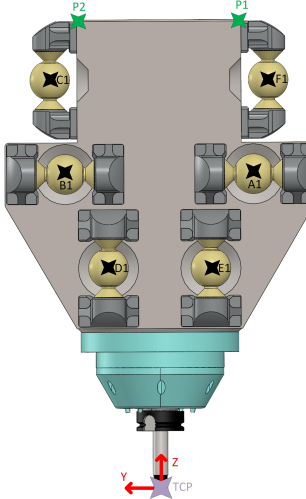


Figure 3.7: Image showing head with relevant points

3.2 Wrist joint

From the previous chapter, it is evident that the most popular solution to making a PKM have more than three DOF is to "cheat" and make it a hybrid mechanism. This is done by adding a one or two DOF wrist joint to the end effector of the PKM, see Figure 3.8.

Parallel designs generally have a combination of high speed good rigidity for how lightweight they are. The drawbacks are that the arms will crash into each other or things without careful mechanical and control systems design. Linear designs are easier to design and will rarely have problems with colliding with itself. Drawbacks are lack of rigidity even though they tend to be on the heavy side. Adding a serial head to a parallel machine allows all the work done to design the parallel machine to be kept while adding the necessary DOFs. This will generally allow you to somewhat play to the strengths of these two designs without too many compromises. This particular wrist joint has the ability to spin 360° in the main joint and ±90° in the secondary joint. Other designs with a different movement possibilities are of course possible, and is also available from multiple different

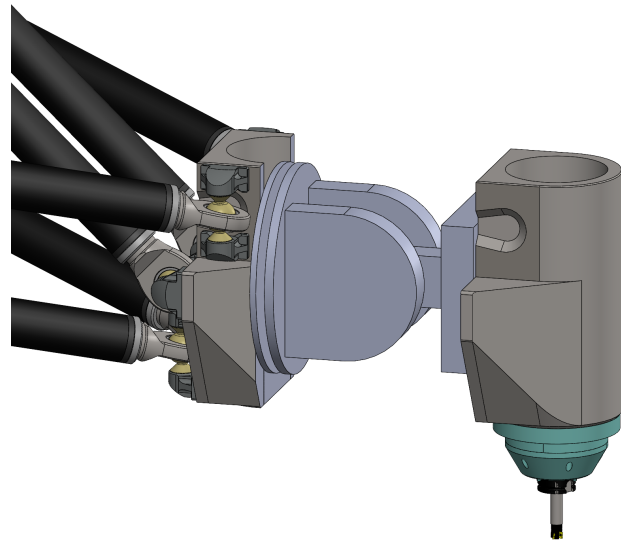


Figure 3.8: Concept model of a wrist joint solution

vendors and will therefore not be considered more in this paper. It is however a quick but mediocre solution to the problem described in the introductory chapter 1. It is mentioned briefly, but will not be considered further, because this solution is already fully tested and available from multiple distributors.

3.3 Extending links

A very popular way to increase the degrees of freedom in PKMs is to have linear actuators that change the length of the linkages. The concept involves exchanging one of the fixed length linkages in our system with an actuated extending linkage. In this report only linkages C and F will be extending, as explained further on. This is a very standard way to achieve the extra degrees of freedom as seen multiple times in chapter 2. This concept has the possibility of being very promising, depending on how long the extension of the links will have to be.

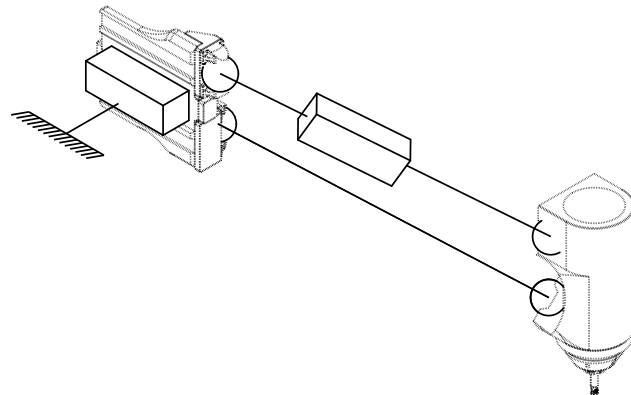


Figure 3.9: Partial diagram of the extending links concept

The inverse kinematic solution of this concept is exactly the same as the system as is, seen in equations 3.1 and 3.2. The major difference being that the point not being calculated using the spherical equation will be the expanding joint and will have mathematically infinite length L in both directions.

3.4 Rotational sleds

Another solution to achieve rotational degrees of freedom is to add a revolute joint to the sleds, see Figure 3.10. The rotational sled concept is interesting because it allows the work that went into the original system to be intact, while the sled is added upon slightly.

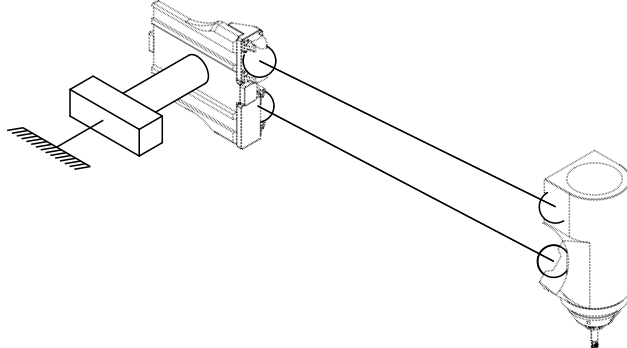


Figure 3.10: Partial diagram of the rotational sled concept

The inverse kinematics of the concept will be explained for east and west sleds, but can be implemented in north sled as well by using A_z instead of A_y . The concept can be thought of as a four bar linkage, but the Center of Rotation (CoR) has a fixed Z-position. Two constant distance constraints are used to control two degrees of freedom, Rotation of the sled and X-position of the sled. The equation to be solved is 3.4, where S_n and S_m are defined by equation 3.3.

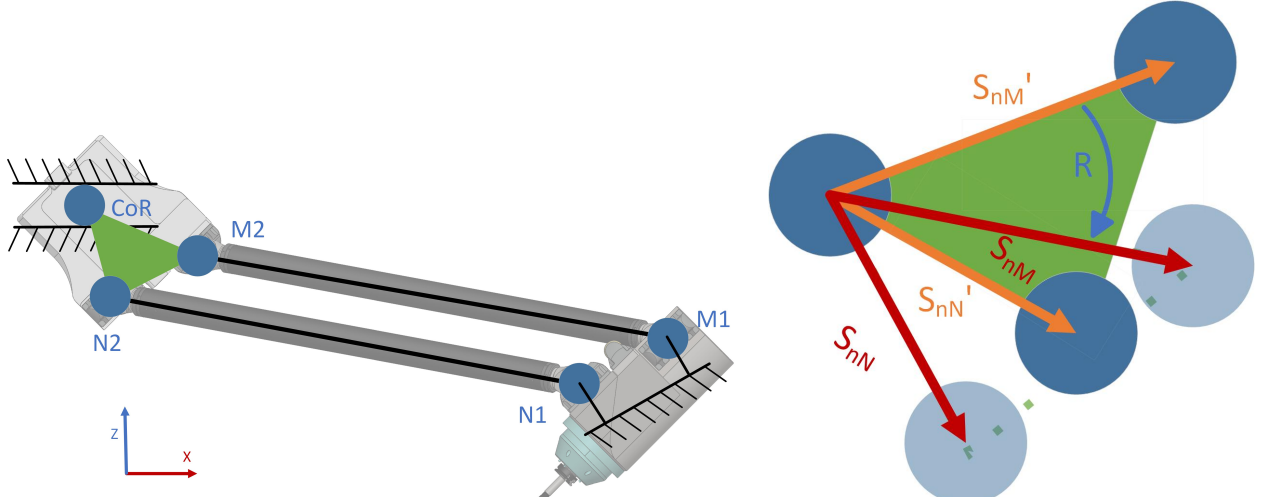


Figure 3.11: Diagram showing the four bar linkage of the rotational sled

Figure 3.12: Rotational sled positional diagram

$$S_n = A_y(R) \cdot S'_n = \begin{bmatrix} \cos(R) \cdot S'_{nx} + \sin(R) \cdot S'_{nz} \\ S'_{ny} \\ -\sin(R) \cdot S'_{nx} + \cos(R) \cdot S'_{nz} \end{bmatrix} \quad (3.3)$$

$$\begin{aligned}
L^2 &= (N2_x - N1_x)^2 + (N2_y - N1_y)^2 + (N2_z - N1_z)^2 \\
L^2 &= (CoR_x + S_{nNx} - N1_x)^2 + (CoR_y + S_{nNy} - N1_y)^2 + (CoR_z + S_{nNz} - N1_z)^2 \\
&\quad \downarrow \\
CoR_x &= N1_x - S_{nNx} - \sqrt{L^2 - (CoR_y + S_{nNy} - N1_y)^2 - (CoR_z + S_{nNz} - N1_z)^2} \\
&= \\
M1_x - S_{nMx} &- \sqrt{L^2 - (CoR_y + S_{nMy} - M1_y)^2 - (CoR_z + S_{nMz} - M1_z)^2}
\end{aligned} \tag{3.4}$$

Equation 3.4 has no algebraic solution since it contains both sine and cosine of angle R. Thus a one dimensional Newton-Raphson solver is used to find the solution. For a pure Y-direction rotation, the angle R of the sled is equal to angle py of the head. This is due to symmetry of the joint positions, and will not be true if any of the values on the head, sled or linkages are changed. In this report this short cut is used where possible to save computer cycles. The derived dR used in the NR solver can be seen in equation 3.5, but will not be proven further in this report. The Newton-Raphson solver implemented in Matlab code can be found in Appendix E.4.

$$\begin{aligned}
\frac{d3.4}{dR} &= -\frac{dS_{nNx}}{dR} - \frac{df_1}{df_2} + \frac{dS_{nMx}}{dR} + \frac{df_3}{df_4} \\
&\quad \text{where} \\
df_1 &= \frac{dS_{nNz}}{dR} (CoR_z + S_{nNz} - N1_z) \\
df_2 &= \sqrt{L^2 - (CoR_y + S_{nNy} - N1_y)^2 - (CoR_z + S_{nNy} - N1_z)^2} \\
df_3 &= \frac{dS_{nMz}}{dR} (CoR_z + S_{nMz} - M1_z) \\
df_4 &= \sqrt{L^2 - (CoR_y + S_{nMy} - M1_y)^2 - (CoR_z + S_{nMy} - M1_z)^2} \\
\frac{dS_{nNx}}{dR} &= -\sin(R) \cdot S'_{nx} + \cos(R) \cdot S'_{nz} \\
\frac{dS_{nNz}}{dR} &= -\cos(R) \cdot S'_{nx} - \sin(R) \cdot S'_{nz}
\end{aligned} \tag{3.5}$$

3.5 Revolute frame

Another solution could be to redesign the frame to include a revolute joint to allow the main translational joints to rotate around the center point of the frame. This will allow one rotational degree of freedom for the end effector. This scheme will only provide rotation around the x-axis. The other direction can be accomplished by for example by implementing the rotational sled concept on both the east and west sleds.

This concept is interesting but would require a lot of redesign for barely being able to partially machine three sides of the work piece. It could be implemented along with any of the other concepts listed in this chapter, but then why have redundant actuating joints in the system? The other concepts listed here can handle 4 sided machining for at least part of the work space. The concept also involves moving a large amount of mass which means the speed of the head will probably suffer greatly. For these reasons this concept is dropped and will not be mentioned further in the report.

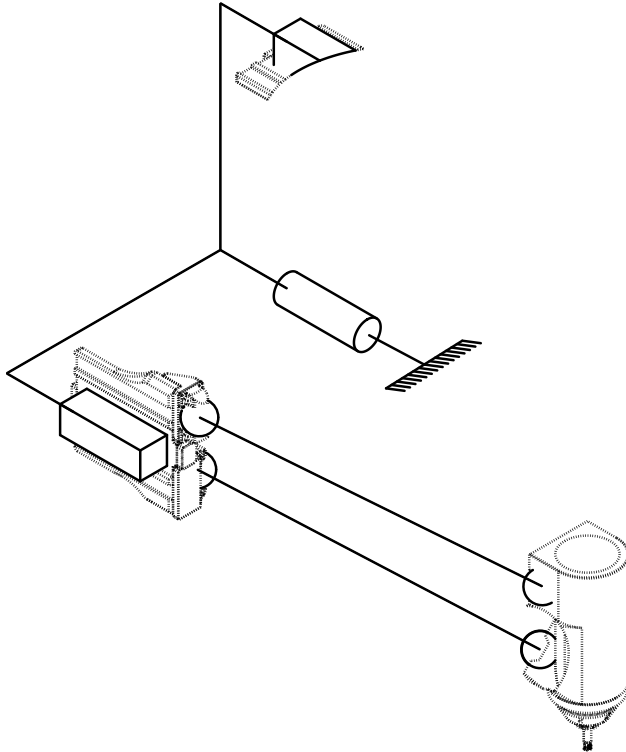


Figure 3.13: Partial diagram of the rotational frame concept

3.6 Revolute gantry

Another possible concept is to add a rotational joint between the frame and the gantry, see Figure 3.14. This concept is the same as the rotational sled concept, but the rotational joint comes before the translational joint in the order of operations. This means that the rotational joint of this concept gets more effect on the head than the rotational sled concept since any rotation is amplified by the translation of the sled increasing the arm.

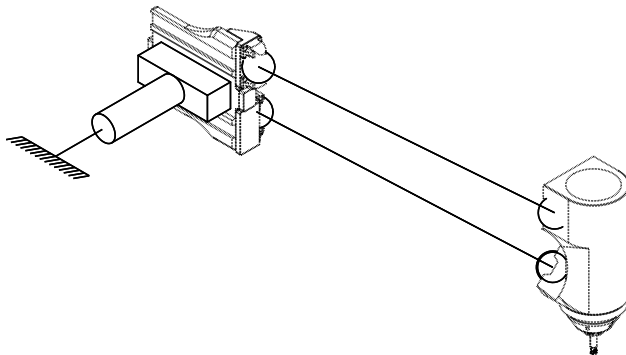


Figure 3.14: Partial diagram of the rotational frame concept

The concept compared to the rotational frame concept has more possible rotation of the head for a smaller change of angle at the joint. This is due to the translational joint magnifying the effect of the rotational joint. It does however fail to be modular. Any change to the length of the gantry will require all graphs referring to strength and work space to have to be recalculated. Also having a 3 meter wide gantry swinging wildly during operation would be quite a large health and safety concern. It would take either take a large amount of engineering to make it run quick safely, or it would be necessary to make it run slowly thereby nullifying the advantage of the PKM design. This means the concept is discarded and will not be checked further in this report.

3.7 Delta light concept

A Delta picker machine will change the effective length of its arms by collapsing a knee joint on its arm or base. This is a system that is too flexible for use on a CNC machine but the idea can be adapted. Adding a rotational joint on the sled connected to an arm that has a ball socket joint at the end will function similar to a delta picker robot. This allows the effective length of the arm to be varied based on the rotational position of the base joint. To increase stiffness of the concept the arm will probably have to be designed like a spinning disk being supported both on its centre and along the edge.

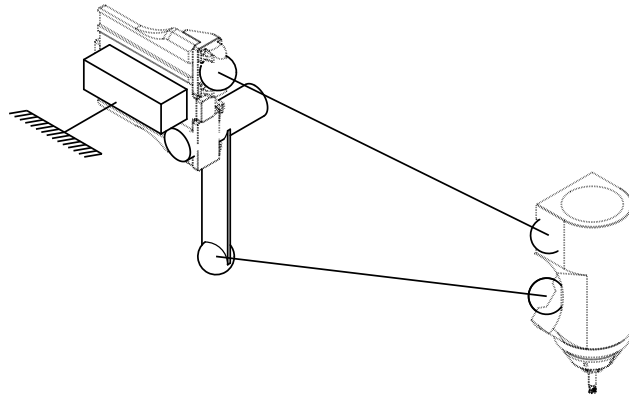


Figure 3.15: Partial diagram showing the delta light concept

Delta concept is very similar to the rotational sleds concept. The main difference is that only one linkage moves in a rotational fashion. This means you have less movable linkage point to cause change of the head rotation, but with a higher degree of stiffness since one linkage is directly mounted to the sled. The concept also means that any development work already done can mostly be kept, while the rotating joint is added to the sled.

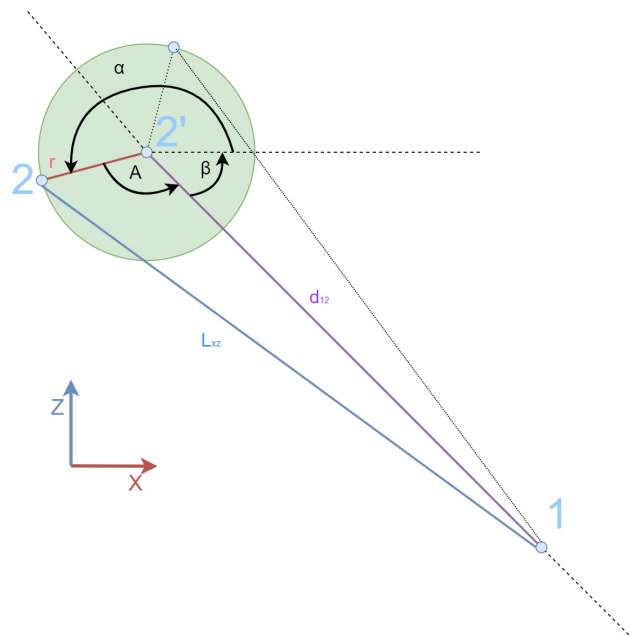


Figure 3.16: Delta light kinematic diagram

The inverse kinematics of the concept is calculated using the shadow of the system in the XZ-plane with the cosine rule for the triangle in Figure 3.16. First the shadow of the link in the XZ-plane

is found using equation 3.6. This length is used to solve the cosine rule in equation 3.8. Finding the joint position requires finding the angle of the in-plane shadow between point 1 and 2' against the X-axis, called β in equation 3.7. Sine is used in this equation because point 1 in Figure 3.16 will move above the point 2' during testing, and that requires the sign of angle beta to change. Finally the joint position is calculated using equation 3.9, which is used in equation 3.10 to find final position of point 2. This kinematic solution has been implemented for the east and west sleds, but can be implemented for north sled by changing Δy to Δz in equation 3.6, and d_{12z} to d_{12y} in equation 3.7. The equations mentioned have also been included in Matlab code in Appendix E.5.

$$L^2 = L_{xz}^2 + \Delta y^2 \rightarrow L_{xz} = \sqrt{L^2 - \Delta y^2} \quad (3.6)$$

$$\beta = \sin^{-1} \left(\frac{d_{12z}}{d_{12}} \right) \quad (3.7)$$

$$A = \cos^{-1} \left(\frac{r^2 + d_{12}^2 - L_{xz}^2}{2 \cdot r \cdot d_{12}} \right) \quad (3.8)$$

$$\alpha = 360^\circ - A - \beta \quad (3.9)$$

$$\begin{aligned} x_2 &= x'_2 + r \cdot \cos(\alpha) \\ z_2 &= z'_2 + r \cdot \sin(\alpha) \end{aligned} \quad (3.10)$$

3.8 Double sled concept

The last concept that will be examined is to have a second sled on the same gantry. Schematic representation of this concept can be seen in Figure 3.17. This can be done by either having one or two tracks. The costs associated with two tracks are quite large but the costs of using a single track is that the linkages become longer and the potential workspace then becomes smaller. Keeping with the spirit of the thesis, it is chosen to make as small a change as possible and therefore it is decided to only consider the single track solution.

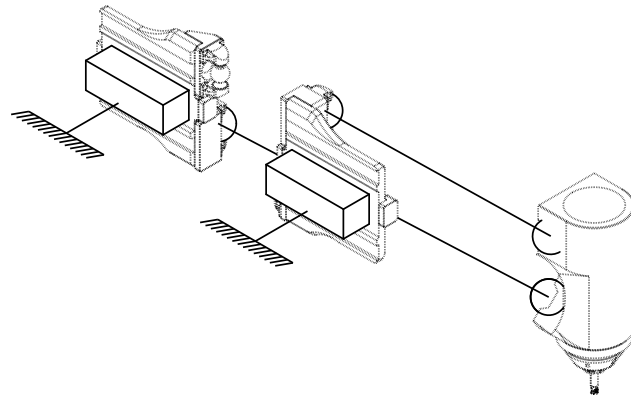


Figure 3.17: Partial diagram showing the double sled concept

The inverse kinematics of this concept is quite simple. It uses two constant distance constraints to find out the two X-coordinates of the two sleds. So the equation to be solved is equation 3.1, only do that for both the linkage fastening points individually.

Chapter 4

Mobility testing

This chapter will explore the maximum possible rotation for each concept, both with and without taking into account crashing of the linkages because of the current design of the head. The chapter will place the TCP in the allowed YZ-space and calculate the maximum possible head rotations for each concept. The concepts have been decided to be distributed one each on the east and west sled with the north sled being left as is, see Figure 3.5. This is because the north sled should be as rigid as possible to withstand the moment coming from the rotation of the TCP against the work piece. Having a joint in this sled would introduce lag between the tool point changing pressure on the work piece and the actuator in the north sled countering the resulting moment. This would introduce a serious accuracy problem and is thus considered a bad idea. Having several actuators in east and west sleds, i.e. redundant actuation, is also avoided since the spirit of this paper is to document the effect of as small a change as possible. Redundant actuation might have a place in this system, but that decision will have to come at a later stage.

4.1 Testing scheme

This chapter will detail the testing criteria for the mobility tests. Having concept joints only in the east and west sleds means it is possible to achieve a pure Y-rotation and a combination XZ-rotation. The largest possible X and Y rotation the kinematics can be solved for will be graphed in the positive and negative directions resulting in four graphs for each concept tested.

Maximum positive Y direction rotation will check when Linkages A and B no longer can be solved for using real values. Negative Y rotation will test for when the links connected to north sled touches the top of the head, see Figure 4.1. The if-test logic used to achieve this can be seen in pseudocode below this paragraph with accompanying diagram in Figure 4.2. Note that all distance values are scalars. Distance D_{Pn} is calculated using a formula for distance between a point and a line, equation 4.1, where P is the point, and P_1 is a point on the line and v_1 is any vector along the line. Distance d_P is calculated using equation 4.2 for distance between two lines, where input values are any point P_n and any vector v_n on each line. The functions implemented in Matlab code can be found in Appendix E.2.

```
if d_P1 < r or d_P2 < r
    break
elseif d_P < r and d_P1 < d_P12 and d_P2 < d_P12
    break
else
    plot results
end
```

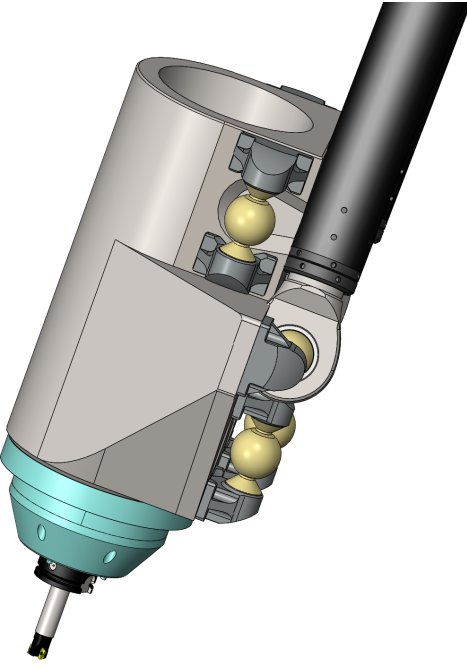


Figure 4.1: Negative Y-rotation maximum travel

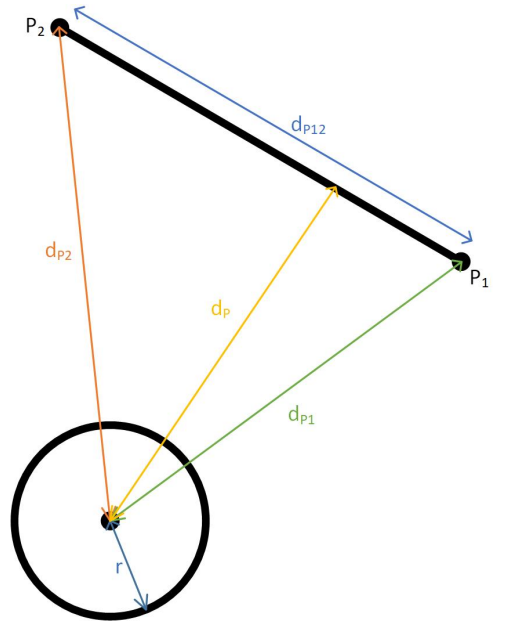


Figure 4.2: Diagram showing how impact is calculated in negative Y-direction

$$d_{pl} = \left| \frac{(P_1 - P) \times v_1}{|v_1|} \right| \quad (4.1)$$

$$d_{ll} = \left| \frac{(v_1 \times v_2) \cdot (P_2 - P_1)}{|v_1 \times v_2|} \right| \quad (4.2)$$

To achieve rotation in X-direction, a combination of X and Z-direction has to be allowed since a third actuator on the north sled is needed to have a pure X-direction rotation. By increasing the X-rotation of the head, this results in both a necessary Z-rotation of the head as well as change of X-position of the north sled. This rotation of the head and translation of the north sled is controlled by the two constant distance constraints A and B. The constant distance constraint is defined by the spherical equation seen in equation 4.3. The head point coordinates for positions A1 and B1 are found using Bryant angles X-Z, and can be seen in equation 4.4.

$$L^2 = (X_{end} - X_{start})^2 + (Y_{end} - Y_{start})^2 + (Z_{end} - Z_{start})^2 \quad (4.3)$$

$$\begin{aligned} X &= \text{TCP}_x + X' \cos(\text{pz}) - Y' \sin(\text{pz}) \\ Y &= \text{TCP}_y + X' \cos(\text{px}) \sin(\text{pz}) + Y' \cos(\text{px}) \cos(\text{pz}) - Z' \sin(\text{px}) \\ Z &= \text{TCP}_z + X' \sin(\text{px}) \sin(\text{pz}) + Y' \sin(\text{px}) \cos(\text{pz}) + Z' \cos(\text{px}) \end{aligned} \quad (4.4)$$

The parameters of the head orientation are not linear due to both sine and cosine being in the equation and will therefore be solved using a Newton-Raphson solver. This means that the equation to be solved is equation 4.5. The specifics of the derivation shall not be shown here, but the derived of this equation with regards to head angle pz can be seen in equation 4.6 and 4.7. Pseudocode of the break conditions when the equation no longer returns a valid solution can be seen below as well. The Newton-Raphson solver implemented in Matlab code can be found in Appendix E.3.

$$\begin{aligned}
A1_x - f_1 &= B1_x - f_2 \\
\downarrow \\
f(pz) &= A1_x - f_1 - B1_x + f_2
\end{aligned} \tag{4.5}$$

where

$$\begin{aligned}
f_1 &= \sqrt{L^2 - (A2_y - A1_y)^2 - (A2_z - A1_z)^2} \\
f_2 &= \sqrt{L^2 - (B2_y - B1_y)^2 - (B2_z - B1_z)^2}
\end{aligned}$$

$$\begin{aligned}
\frac{df}{dpz} &= \frac{A1_x}{dpz} + \frac{df_1}{df_2} - B1_x - \frac{df_3}{df_4} \\
&\quad \text{where} \\
df_1 &= \frac{dA1_y}{dpz}(A1_y - A2_y) + \frac{dA1_z}{dpz}(A2_z - A1_z) \\
df_2 &= \sqrt{L^2 - (A2_y - A1_y)^2 - (A2_z - A1_z)^2} \\
df_3 &= \frac{dB1_y}{dpz}(B2_y - B1_y) + \frac{dB1_z}{dpz}(B1_z - B2_z) \\
df_4 &= \sqrt{L^2 - (B2_y - B1_y)^2 - (B2_z - B1_z)^2}
\end{aligned} \tag{4.6}$$

$$\begin{aligned}
\frac{dx}{dpz} &= -X' \sin(pz) - Y' \cos(pz) \\
\frac{dy}{dpz} &= X' \cos(px) \cos(pz) - Y' \cos(px) \sin(pz) \\
\frac{dz}{dpz} &= X' \sin(px) \cos(pz) + Y' \sin(px) \sin(pz)
\end{aligned} \tag{4.7}$$

```

if NOT isreal(pz)
    break
elseif NOT isreal(D2_x+C2_x)
    break
else
    plot results
end

```

A further two graphs will show the largest possible X-rotations while the links also do not touch each other. It is of course possible to stop the links touching by increasing the size of the head. The larger head would however decrease the possible applications of the finished product because it needs more room to maneuver. It might however be possible to slightly change the dimensions and gain a large increase in the possible work space. Thus the two sets of graphs are meant to be compared against each other. The added parameters to be checked is that the distance between the two center lines of the linkages does not become smaller than a diameter of the linkage, using equation 4.2. This check will be added to the checks specified previously in the chapter.

4.2 Extending links

This chapter will show maximum possible head rotation using the extending links concept in the linkages C and F.

4.2.1 Pure kinematic potential in all directions

This sub chapter will show the absolute maximum head rotation using this concept. Kinematic potential in Y-direction can be seen in Figures 4.3 and 4.4. Kinematic potential in X-direction can be seen in Figures 4.5 and 4.6.

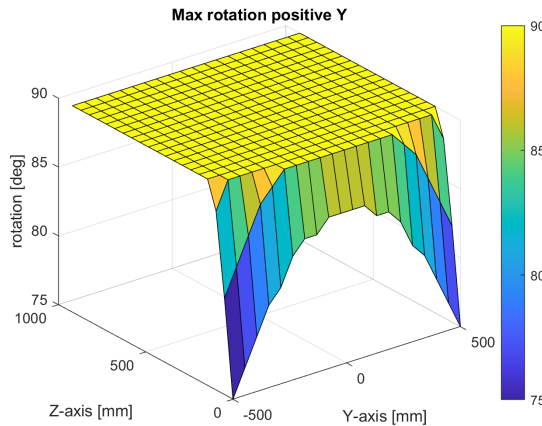


Figure 4.3: Maximum kinematic potential for extending links concept in positive Y-direction

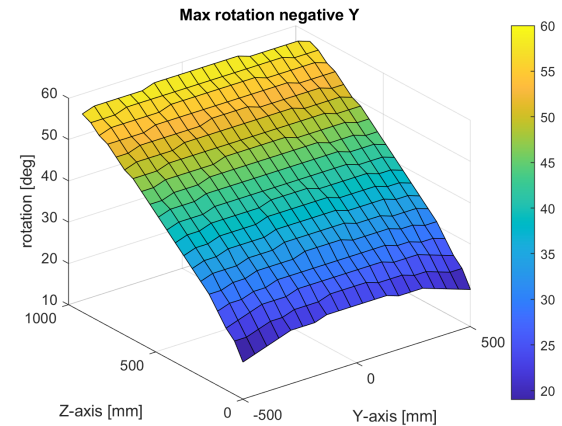


Figure 4.4: Maximum kinematic potential for extending links concept in negative Y-direction

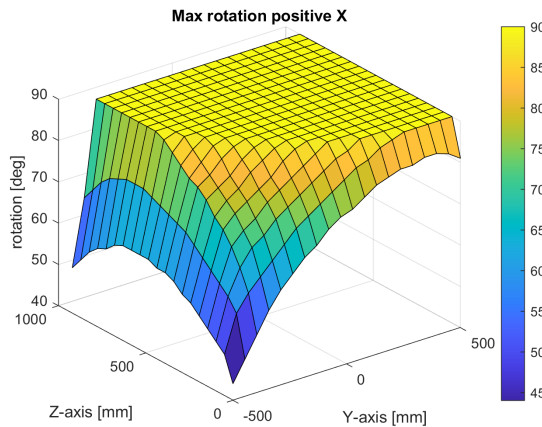


Figure 4.5: Maximum kinematic potential for extending links concept in positive X-direction

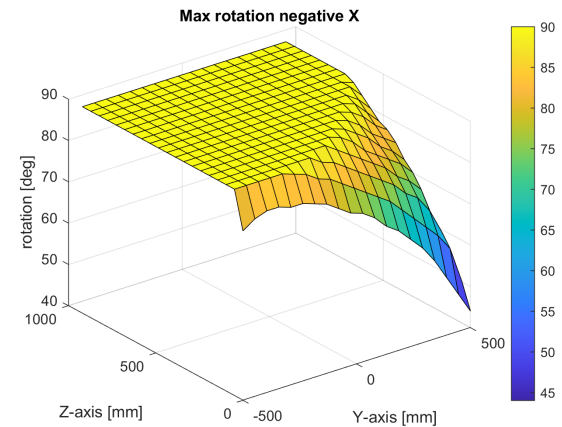


Figure 4.6: Maximum kinematic potential for extending links concept in negative X-direction

4.2.2 Kinematic potential while taking linkage geometry into account in X-rotation

This sub chapter will show the maximum head rotation in X-direction while not colliding with the linkages. The figures can be seen in Figure 4.7 and 4.8.

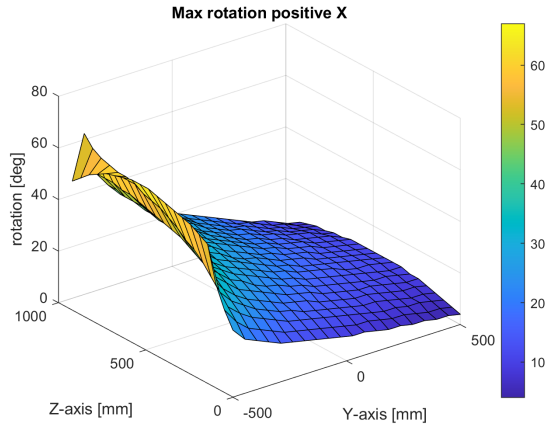


Figure 4.7: Max possible rotation positive X while taking into account impact of linkages

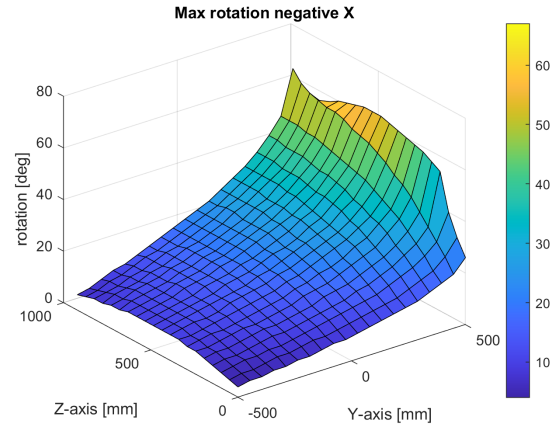


Figure 4.8: Max possible rotation neg X while taking into account impact of linkages

4.3 Delta Light

This chapter will show maximum possible head rotation using the delta light concept in the sled fastening of linkages D and E.

4.3.1 Pure kinematic potential in all directions

This sub chapter will show the absolute maximum head rotation using this concept. Kinematic potential in Y-direction can be seen in Figures 4.9 and 4.10. Kinematic potential in X-direction can be seen in Figures 4.11 and 4.12.

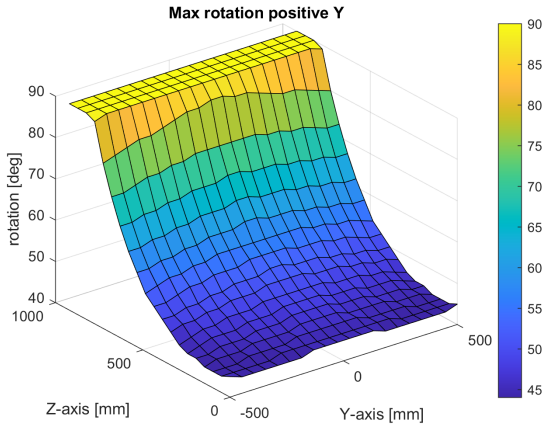


Figure 4.9: Maximum kinematic potential for delta light concept in positive Y-direction

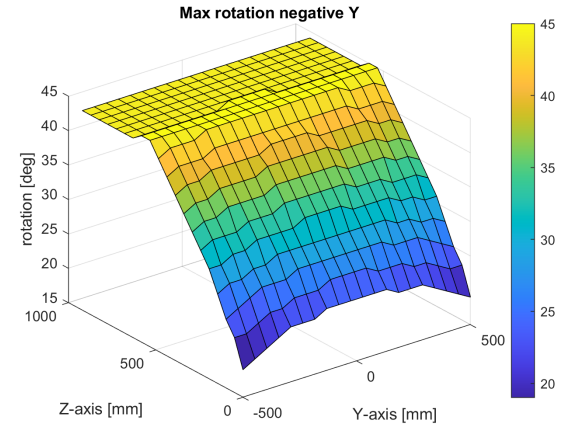


Figure 4.10: Maximum kinematic potential for delta light concept in negative Y-direction

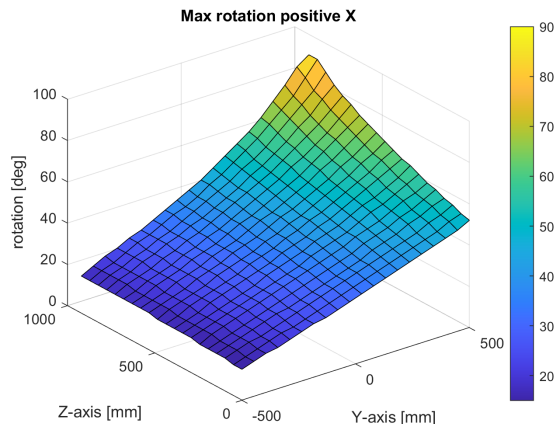


Figure 4.11: Maximum kinematic potential for delta light concept in positive X-direction

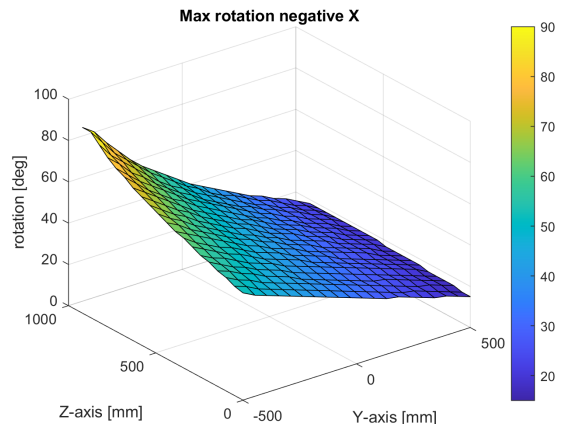


Figure 4.12: Maximum kinematic potential for delta light concept in negative X-direction

4.3.2 Kinematic potential while taking linkage geometry into account in X-rotation

This sub chapter will show the maximum head rotation in X-direction while not colliding with the linkages. The figures can be seen in Figure 4.13 and 4.14.

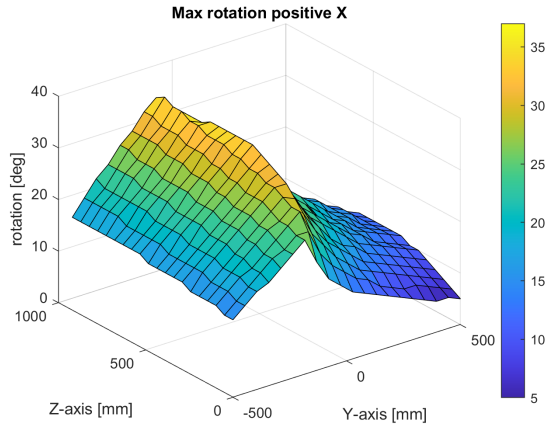


Figure 4.13: Max possible rotation positive X while taking into account impact of linkages

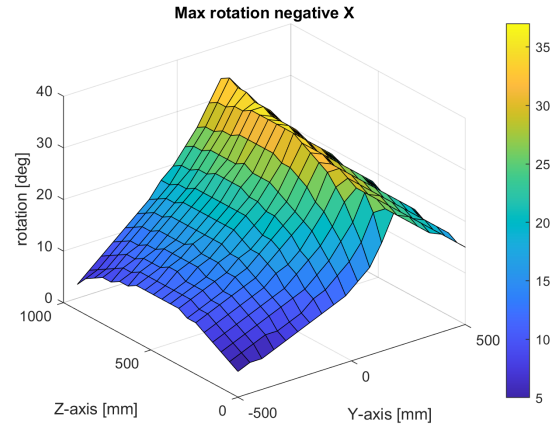


Figure 4.14: Max possible rotation neg X while taking into account impact of linkages

4.4 Rotational sleds

This chapter will show maximum possible head rotation using the rotational sled concept in the east and west sleds.

4.4.1 Pure kinematic potential in all directions

This sub chapter will show the absolute maximum head rotation using this concept. Kinematic potential in Y-direction can be seen in Figures 4.15 and 4.16. Kinematic potential in X-direction can be seen in Figures 4.17 and 4.18.

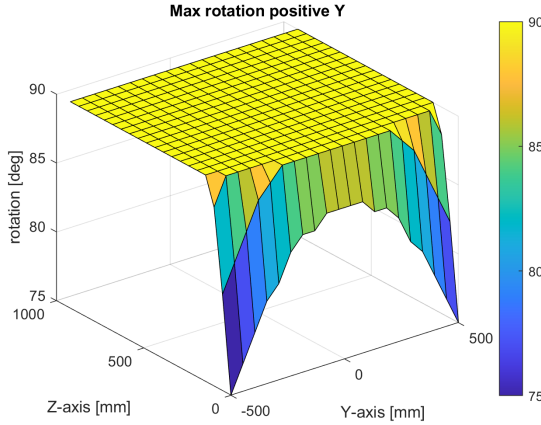


Figure 4.15: Maximum kinematic potential for rotational sled concept in positive Y-direction

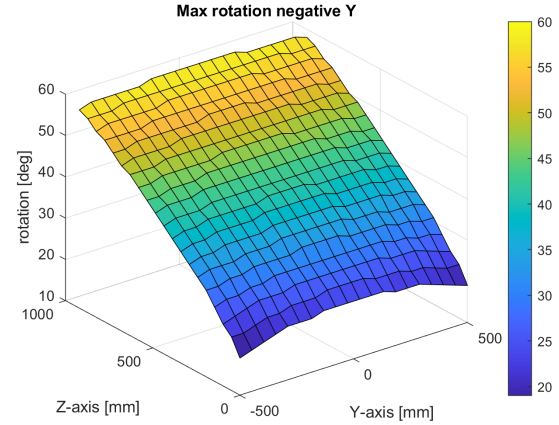


Figure 4.16: Maximum kinematic potential for rotational sled concept in negative Y-direction

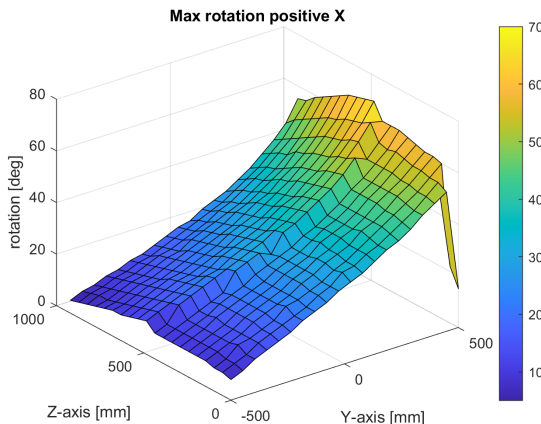


Figure 4.17: Maximum kinematic potential for rotational sled concept in positive X-direction

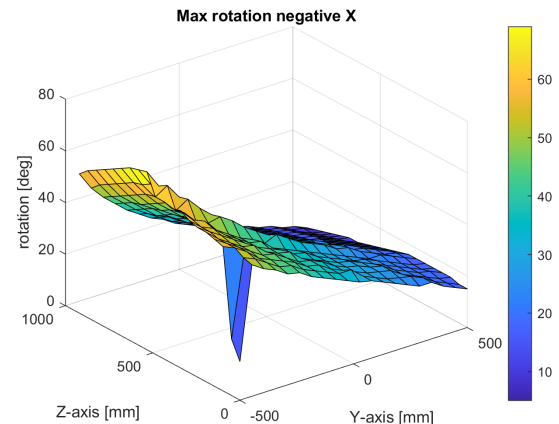


Figure 4.18: Maximum kinematic potential for rotational sled concept in negative X-direction

4.4.2 Kinematic potential while taking linkage geometry into account in X-rotation

This sub chapter will show the maximum head rotation in X-direction while not colliding with the linkages. The figures can be seen in Figure 4.19 and 4.20.

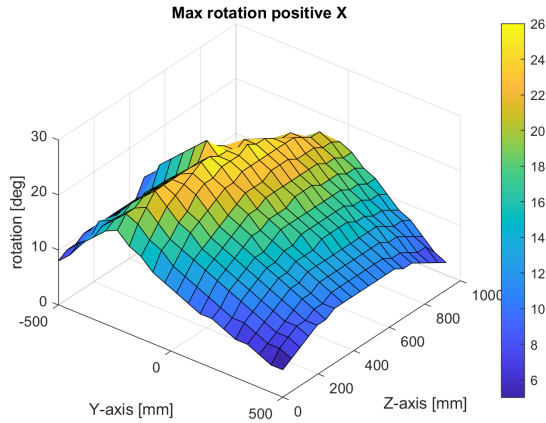


Figure 4.19: Max possible rotation positive X while taking into account impact of linkages

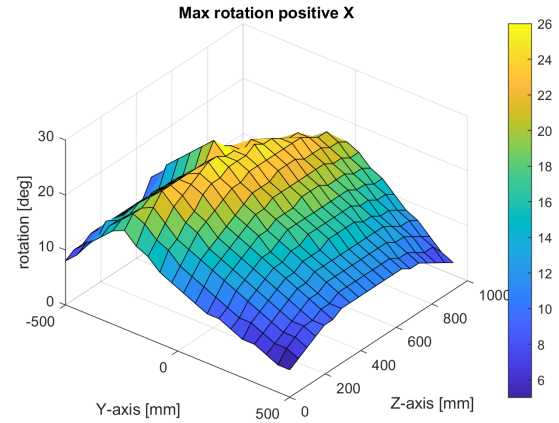


Figure 4.20: Max possible rotation neg X while taking into account impact of linkages

4.5 Double Sled

This chapter will show maximum possible head rotation using the double sled concept in the east and west sleds.

4.5.1 Pure kinematic potential in all directions

This sub chapter will show the absolute maximum head rotation using this concept. Kinematic potential in Y-direction can be seen in Figures 4.21 and 4.22. Kinematic potential in X-direction can be seen in Figures 4.23 and 4.24.

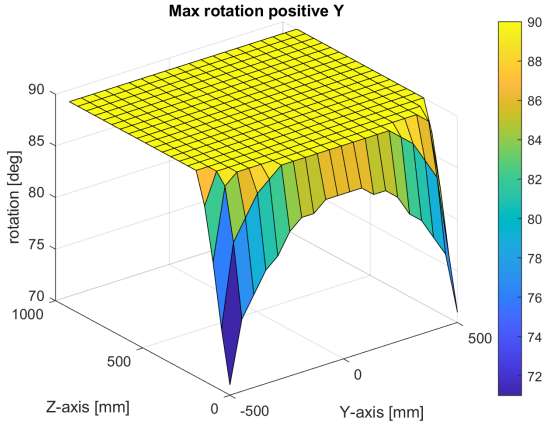


Figure 4.21: Maximum kinematic potential for double sled concept in positive Y-direction

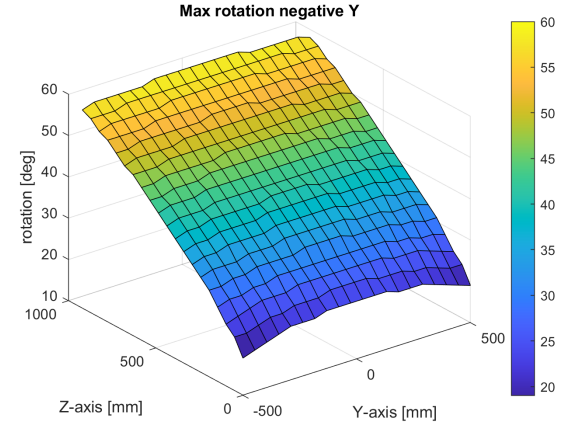


Figure 4.22: Maximum kinematic potential for double sled concept in negative Y-direction

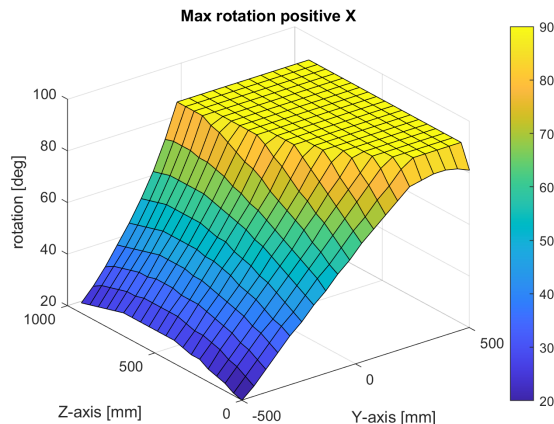


Figure 4.23: Maximum kinematic potential for double sled concept in positive X-direction

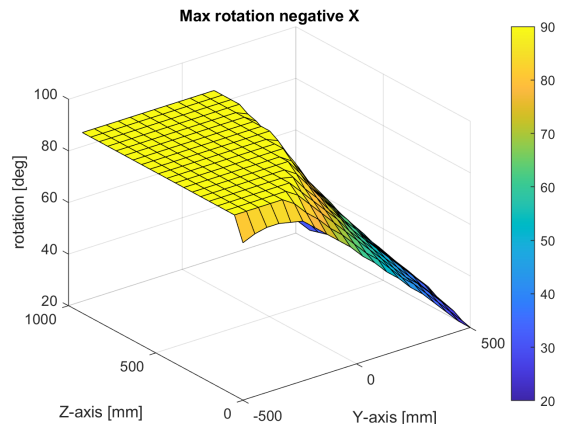


Figure 4.24: Maximum kinematic potential for double sled concept in negative X-direction

4.5.2 Kinematic potential while taking linkage geometry into account in X-rotation

This sub chapter will show the maximum head rotation in X-direction while not colliding with the linkages. The figures can be seen in Figure 4.25 and 4.26.

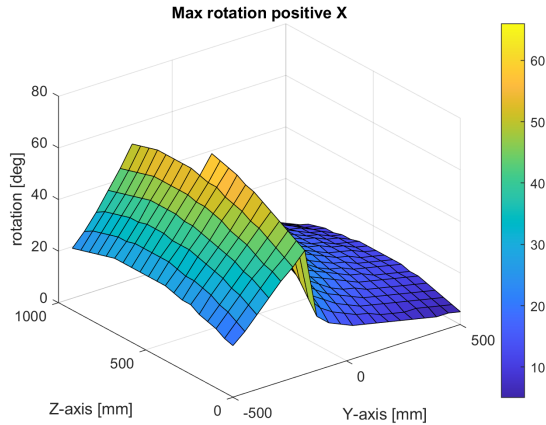


Figure 4.25: Max possible rotation positive X while taking into account impact of linkages

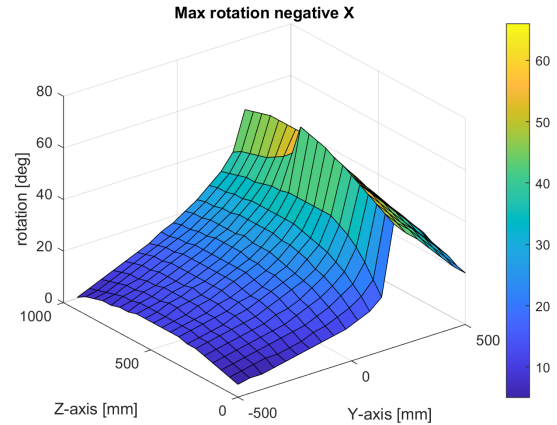


Figure 4.26: Max possible rotation neg X while taking into account impact of linkages

4.6 Discussion

In this chapter the possible movement of all the concepts shall be assessed for potential further on in the report. Since they all look very similar the discussion will be centralized to a single chapter.

In general it can be observed that rotation in the negative Y-direction is very similar for all concepts and can be discounted as a legitimate possibility for further development due to the lackluster results. The linkages hit the head very similarly for all concepts, managing between 20° and 60°, and would need major redesign of the head to be even remotely viable. Further it can be seen that the X-direction shows promise in a few of the concepts. Namely extending links and double sled concepts where it is possible to rotate 90° in about half the workspace. Unfortunately, when taking into account the impacts with the linkages, this direction also falls flat, only managing about 20° in about half the workspace. It is possible to redesign the head to be bigger and thus avoid collisions, but at this stage of the report that is not an option. However there is a direction that bears potential for all concepts. Positive Y-direction has the ability to achieve 90° for at least the top part of the workspace for all concepts. Therefore it is decided that this direction will be investigated further on in the report as the only viable direction.

Chapter 5

Stiffness and Singularity Testing

PKMs are very dependant on the stiffness of the system of joints. This chapter aims to test the different concepts against each other primarily on the basis of system stiffness. The head will be able to withstand forces at the end effector differently based on how the linkages are oriented to the forces applied. This chapter will place the end effector with a pre-determined orientation in the entire workspace, and record the stiffness results for forces oriented in the three cardinal directions. As was concluded in Chapter 4, the only rotation that will be considered is going to be positive Y. The script will also include a check for singularities at the chosen position and orientation. Any values reading zero in all the graphs is a position where no joint combination could be calculated because the joint schema physically cannot move there at that head angle in these three dimensions.

5.1 Simplified stiffness calculation method

This chapter will detail the method for testing the stiffness of the system against forces at the TCP. An example of this method implemented can be found in Appendix E.1.

A very accurate model of the stiffness can be accomplished using a 4 or 6-DOF FEM calculation for all linkages. The method chosen however is much more computationally cheap and is taken from Tyapin & Hovland 2011 [17]. The method assumes that deflections of the linkages are only in the axial direction because of the number of linkages, and the stiffness is thus only normal stiffness of the linkage. The linkage is made up of a tube of composite material and metal end points (links). FEM analysis has shown in the past that the metal link roughly has a normal stiffness of $300 \text{ N}/\mu\text{m}$. The stiffness of the composite tube is calculated using equation 5.2, where A is Area, E is elasticity module and L is the length between connection points in the linkage, called length of the linkage. Area is calculated using equation 5.1, where d_o is outer diameter and d_i is inner diameter of the tube. The stiffnesses are in series, see Figure 5.1, and thus the equivalent stiffness for the linkage is found using equation 5.3. All necessary values are found in Table 5.1.

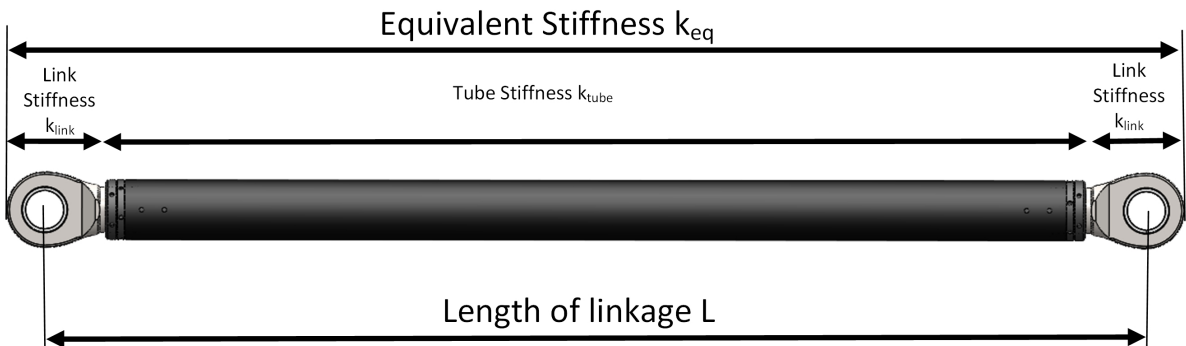


Figure 5.1: Figure showing sectioning and equivalent stiffness of the linkage

$$A = \frac{\pi \cdot (d_o^2 - d_i^2)}{4} \quad (5.1)$$

$$k = \frac{A \cdot E}{(L - 160 \text{ mm})} \quad (5.2)$$

$$\begin{aligned} \frac{1}{k_{eq}} &= \frac{1}{k_{tube}} + 2 \cdot \frac{1}{k_{link}} \\ k_{eq} &= \frac{k_{link} \cdot k_{tube}}{k_{link} + 2 \cdot k_{tube}} \end{aligned} \quad (5.3)$$

Variable	Value
d_o	79 mm
d_i	68 mm
E	180 GPa
L_{short}	1 290 mm
L_{long}	1 400 mm
k_{link}	$300 \frac{N}{\mu m}$
k_{short}	$81.2 \frac{N}{\mu m}$
k_{long}	$78.2 \frac{N}{\mu m}$

Table 5.1: Values and results used in stiffness calculations

As a reminder: 1 denotes linkage connection to head and 2 denotes linkage connection to sled in the equations in this chapter. The equations also uses n for any linkage, i.e $n \in [A, B, \dots, F]$. The method first calculates the directional vector of the linkages, seen in equation 5.4. The method also requires the normal vector of both the linkage and the vector from TCP to the linkage connection on the head, seen in equation 5.5. These two values are collated in equation 5.6 for use in further calculations. Equation 5.7 calculates the stiffness of the six linkages in three directions and three rotations. Though since the method assumes no rotational stiffness, the last three values pr. linkage will be ignored, seen in equation 5.8. Lastly the final stiffness is calculated using equation 5.9, where 1 Newton is divided by the deflections in the first column and three first rows of Δ using a Pythagorean sum.

$$U_n = \frac{n_2 - n_1}{|n_2 - n_1|} \quad (5.4)$$

$$r_n = (n_1 - TCP) \times U_n \quad (5.5)$$

$$H = \begin{bmatrix} U_n & \dots \\ r_n & \dots \end{bmatrix} \quad (5.6)$$

$$\begin{aligned} K_{cart} &= H \cdot I \cdot K \cdot H^T, \\ \text{where } K &= \begin{bmatrix} k_n \\ \vdots \end{bmatrix} \\ \text{and } I \text{ is a } 6x6 \text{ Identity matrix} \end{aligned} \quad (5.7)$$

$$\begin{aligned}
\Delta_x &= K_{cart}^{-1} \cdot [1 \ 0 \ 0 \ 0 \ 0 \ 0]^T \\
\Delta_y &= K_{cart}^{-1} \cdot [0 \ 1 \ 0 \ 0 \ 0 \ 0]^T \\
\Delta_z &= K_{cart}^{-1} \cdot [0 \ 0 \ 1 \ 0 \ 0 \ 0]^T
\end{aligned} \tag{5.8}$$

$$\begin{aligned}
k_x &= \frac{1}{\sqrt{\Delta_{x11}^2 + \Delta_{x21}^2 + \Delta_{x31}^2}} \\
k_y &= \frac{1}{\sqrt{\Delta_{y11}^2 + \Delta_{y21}^2 + \Delta_{y31}^2}} \\
k_z &= \frac{1}{\sqrt{\Delta_{z11}^2 + \Delta_{z21}^2 + \Delta_{z31}^2}}
\end{aligned}, \quad \text{where } \Delta = \begin{bmatrix} \Delta_{11} & \Delta_{12} & \dots \\ \Delta_{21} & \Delta_{22} & \dots \\ \vdots & \vdots & \ddots \end{bmatrix} \tag{5.9}$$

Singularities will be identified by calculating the condition number for matrix inversion of the H matrix from equation 5.6, seen in equation 5.10. Condition numbers will check to which degree the changes to the individual input data will impact the output of a matrix. It is usually used to check for sensitivity to noise and small changes. Here it is used to check whether a small change of input variables will cause a large effect on the output. An infinitely large condition number means a singularity has occurred. A large condition number, meaning a sharp spike in the workspace, means the system has a singularity at that specific point.

$$cond(H) = |H| \cdot |H^{-1}| \tag{5.10}$$

5.2 System as is

Any numbers presented has to be given context. This chapter will show the stiffness of the system as it currently exists in the given directions. Figure 5.2 shows stiffness for forces in X-direction. Figures 5.3 and 5.4 show for forces in Y and Z-direction respectively. Condition number for matrix inversion for system as is can be seen in Figure 5.5. The system as is stiffness computation Matlab script can be found in Appendix E.1.

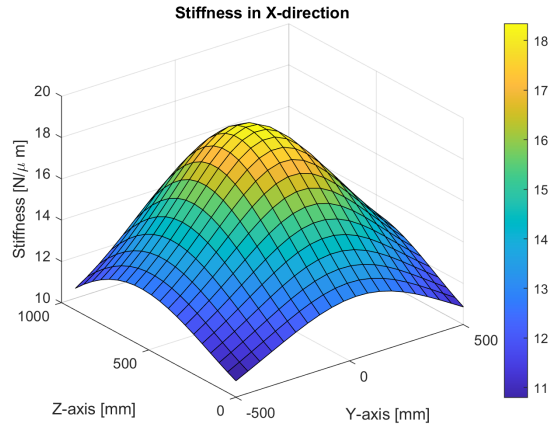


Figure 5.2: Stiffness for system as is for load in X-direction

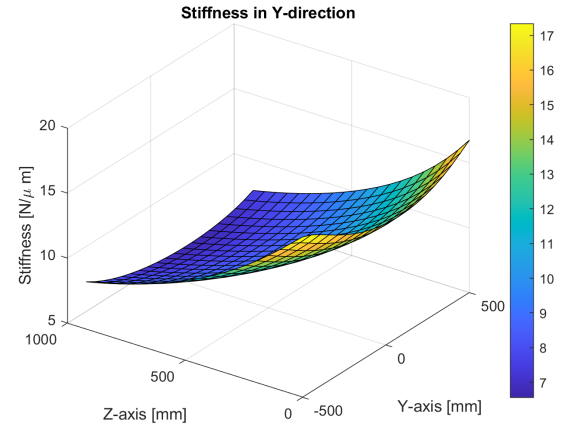


Figure 5.3: Stiffness for system as is for load in Y-direction

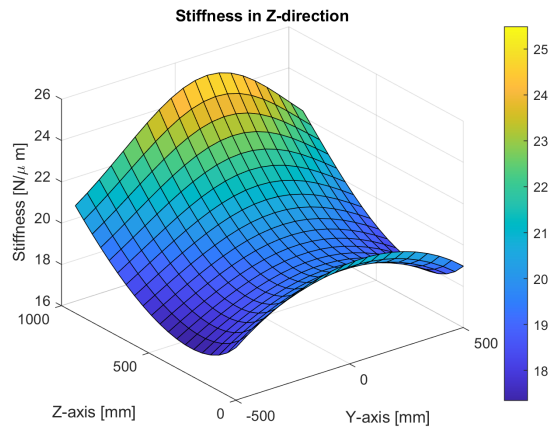


Figure 5.4: Stiffness for system as is for load in Z-direction

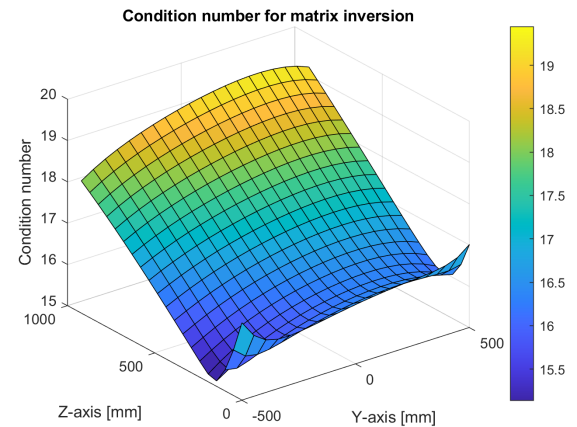


Figure 5.5: System as is condition number for matrix inversion

The values of the stiffness graphs without the zero values included average out to be $14.4 \text{ N}/\mu\text{m}$ in X-direction, $10.3 \text{ N}/\mu\text{m}$ in Y-direction and $20.2 \text{ N}/\mu\text{m}$ in Z-direction.

5.3 Extending links

The following two sub chapters will check the stiffness of the extending links concept for 45° and 90° rotation around Y. Checks for singularity at the position and orientation will also be done. Complete sets of stiffness and singularity graphs can be found in Appendix A.

5.3.1 45 degrees

This sub chapter will show the stiffness and singularity check for the extending links concept at 45° positive Y-angle at the head. Figure 5.6 shows stiffness for forces in X-direction. Figures 5.7 and 5.8 show for forces in Y and Z-direction respectively. Condition number for matrix inversion for system as is can be seen in Figure 5.9.

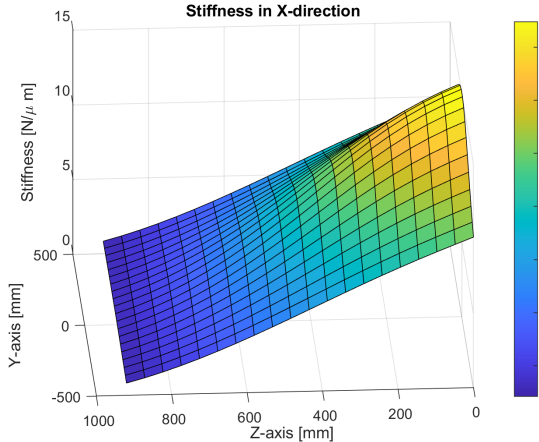


Figure 5.6: Stiffness for extending links at 45 degrees for load in X-direction

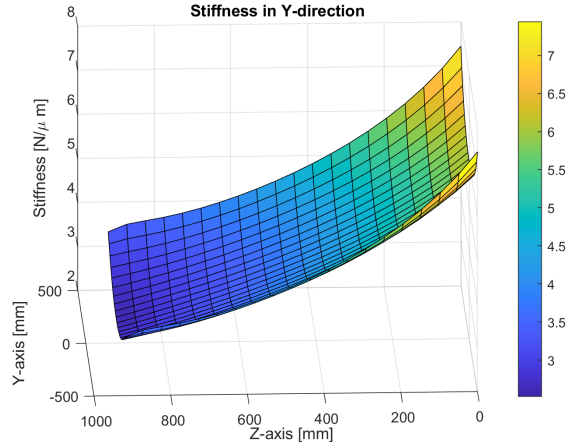


Figure 5.7: Stiffness for extending links at 45 degrees for load in Y-direction

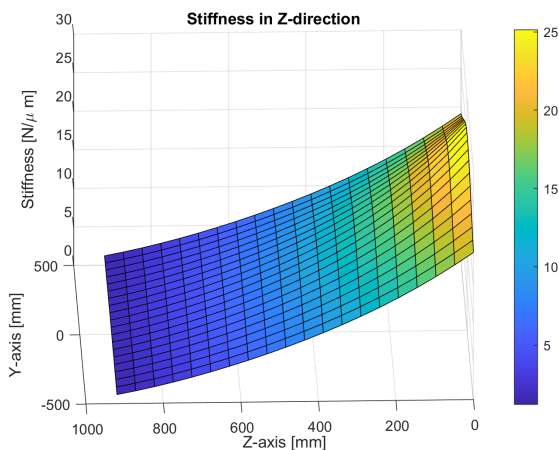


Figure 5.8: Stiffness for extending links in 45 degrees for load in Z-direction

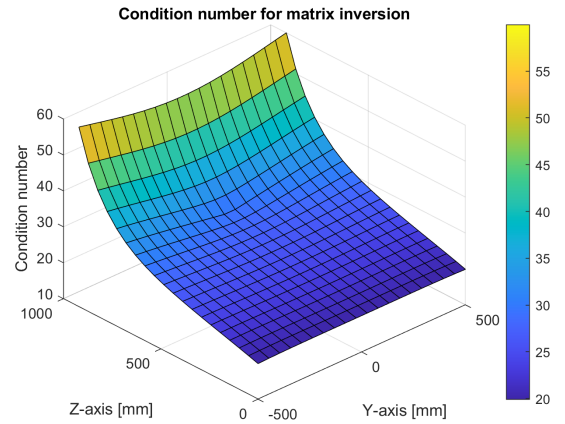


Figure 5.9: Extending links condition number for matrix inversion for extending links concept at 45 degrees head angle

The values of the stiffness graphs without the zero values included average out to be $6.6 \text{ N}/\mu\text{m}$ in X-direction, $4.3 \text{ N}/\mu\text{m}$ in Y-direction and $9.5 \text{ N}/\mu\text{m}$ in Z-direction.

5.3.2 90 degrees

This sub chapter will show the stiffness and singularity check for the extending links concept at 90° positive Y-angle at the head. Figure 5.10 shows stiffness for forces in X-direction. Figures 5.11 and 5.12 show for forces in Y and Z-direction respectively. Condition number for matrix inversion for system as is can be seen in Figure 5.13.

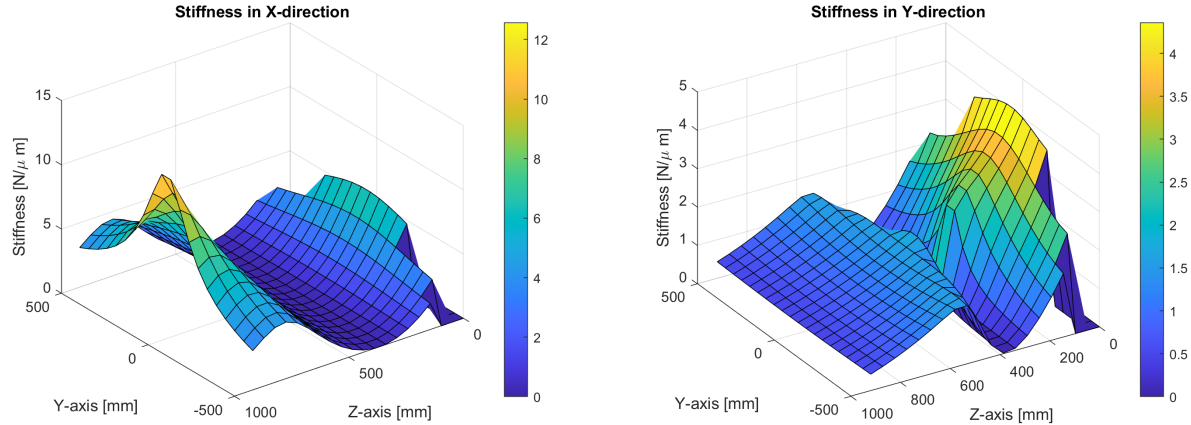


Figure 5.10: Stiffness for extending links for load in X-direction for extending links concept at 90 degrees head angle

Figure 5.11: Stiffness for extending links for load in Y-direction for extending links concept at 90 degrees head angle

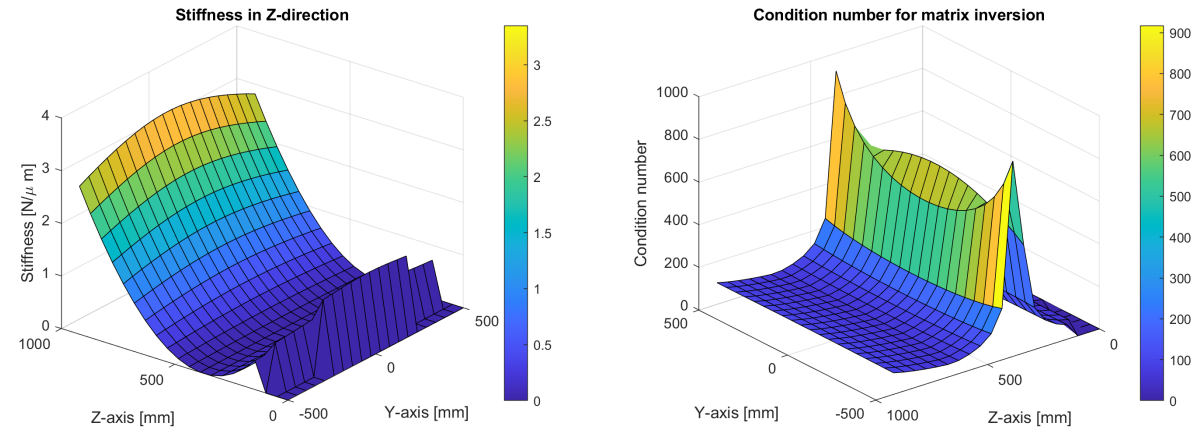


Figure 5.12: Stiffness for extending links for load in Z-direction for extending links concept at 90 degrees head angle

Figure 5.13: Extending links condition number for matrix inversion for extending links concept at 90 degrees head angle

The values of the stiffness graphs without the zero values included average out to be $2.9 \text{ N}/\mu\text{m}$ in X-direction, $1.2 \text{ N}/\mu\text{m}$ in Y-direction and $0.9 \text{ N}/\mu\text{m}$ in Z-direction.

5.4 Rotation sleds

The following two sub chapters will check the stiffness of the rotational sled concept for 45° and 90° rotation around Y. Checks for singularity at the position and orientation will also be done. Complete sets of stiffness and singularity graphs can be found in Appendix B.

5.4.1 45 degrees

This sub chapter will show the stiffness and singularity check for the rotational sleds concept at 45° positive Y-angle at the head. Figure 5.14 shows stiffness for forces in X-direction. Figures 5.15 and 5.16 show for forces in Y and Z-direction respectively. Condition number for matrix inversion for system as is can be seen in Figure 5.17.

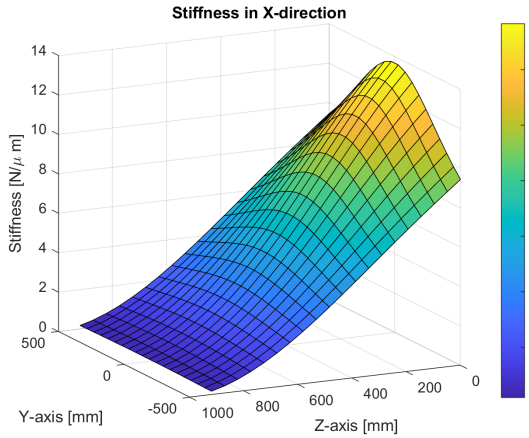


Figure 5.14: Stiffness for rotational sled concept for load in X-direction at 45° head angle

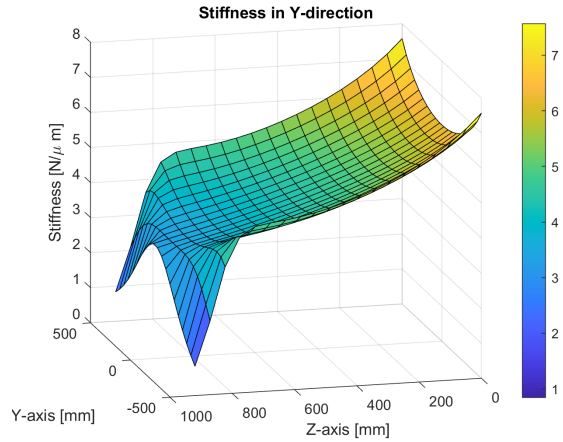


Figure 5.15: Stiffness for rotational sled concept for load in Y-direction at 45° head angle

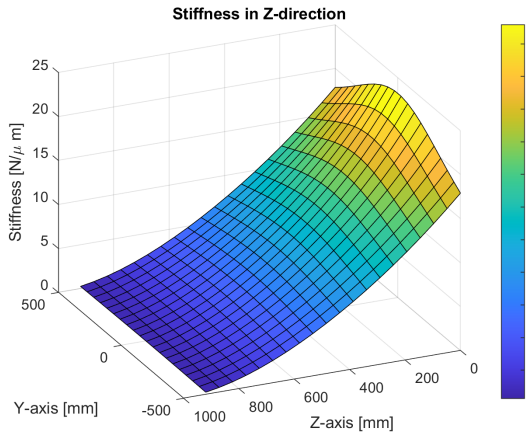


Figure 5.16: Stiffness for rotational sled concept for load in Z-direction at 45° head angle

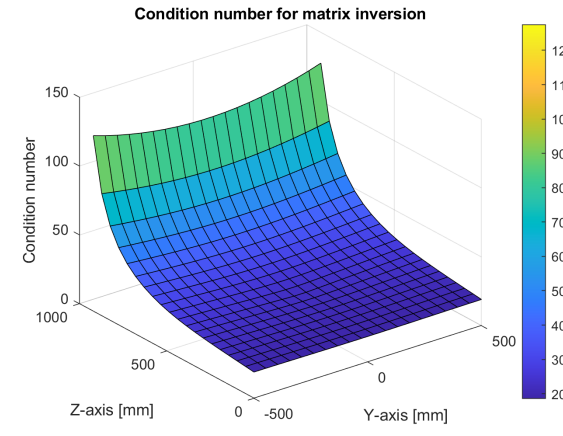


Figure 5.17: Rotational concept condition number for matrix inversion at 45° head angle

The values of the stiffness graphs without the zero values included average out to be $5.2 \text{ N}/\mu\text{m}$ in X-direction, $4.7 \text{ N}/\mu\text{m}$ in Y-direction and $8.2 \text{ N}/\mu\text{m}$ in Z-direction.

5.4.2 90 degrees

This sub chapter will show the stiffness and singularity check for the rotational sleds concept at 90° positive Y-angle at the head. Figure 5.18 shows stiffness for forces in X-direction. Figures 5.19 and 5.20 show for forces in Y and Z-direction respectively. Condition number for matrix inversion for system as is can be seen in Figure 5.21.

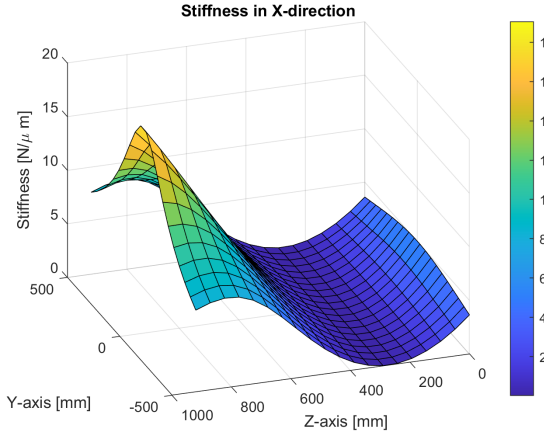


Figure 5.18: Stiffness for rotational sled concept for load in X-direction at 90° head angle

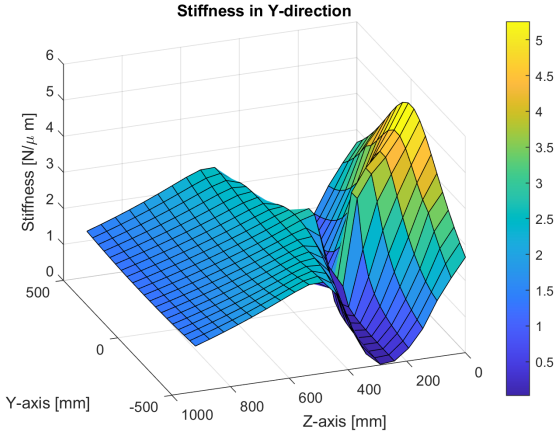


Figure 5.19: Stiffness for rotational sled concept for load in Y-direction at 90° head angle

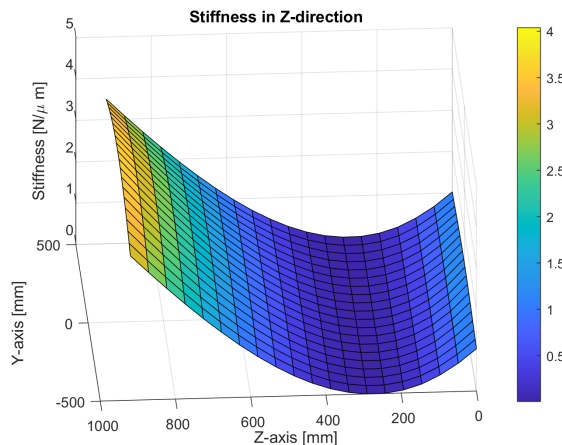


Figure 5.20: Stiffness for rotational sled concept for load in Z-direction at 90° head angle

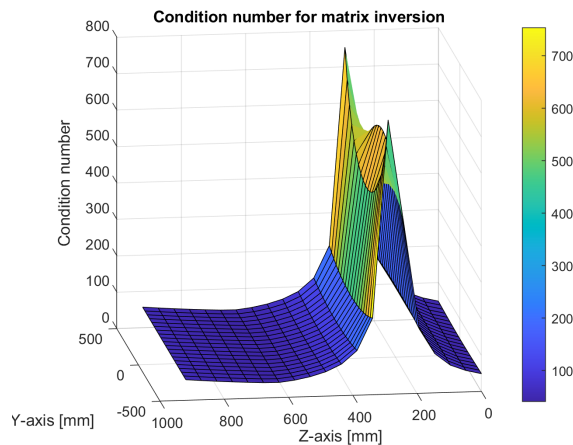


Figure 5.21: Rotational sled concept condition number for matrix inversion at 90° head angle

The values of the stiffness graphs without the zero values included average out to be $4.9 \text{ N}/\mu\text{m}$ in X-direction, $1.8 \text{ N}/\mu\text{m}$ in Y-direction and $1.2 \text{ N}/\mu\text{m}$ in Z-direction.

5.5 Delta light

The following two sub chapters will check the stiffness of the delta light concept for 30° and 45° rotation around Y. The reason these numbers do not correspond to the other sections of this chapter is because the delta light concept does not have the same movement range as the other concepts. Checks for singularity at the position and orientation will also be done. Complete sets of stiffness and singularity graphs can be found in Appendix C.

5.5.1 30 degrees

This sub chapter will show the stiffness and singularity check for the Delta Light concept at 30° positive Y-angle at the head. Figure 5.22 shows stiffness for forces in X-direction. Figures 5.23 and 5.24 show for forces in Y and Z-direction respectively. Condition number for matrix inversion for system as is can be seen in Figure 5.25.

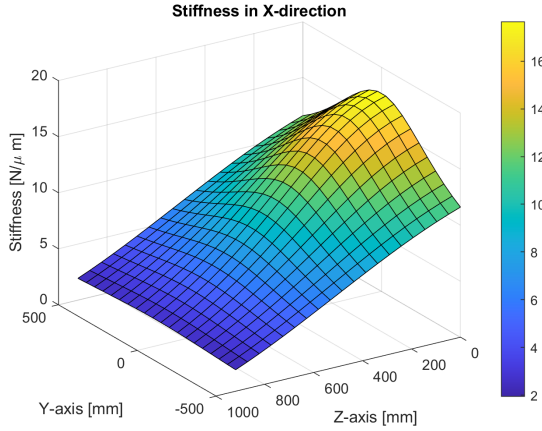


Figure 5.22: Stiffness for delta light concept for load in X-direction at 30° head angle

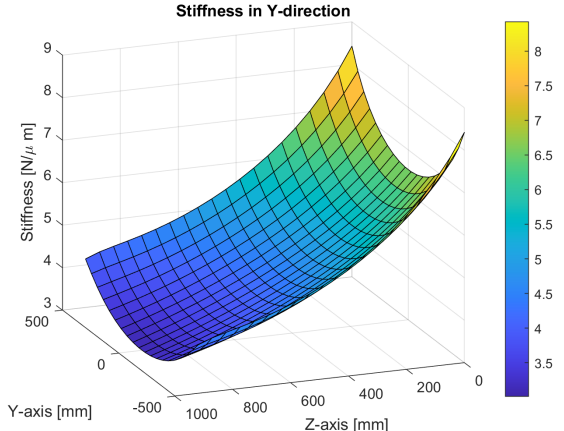


Figure 5.23: Stiffness for delta light concept for load in Y-direction at 30° head angle

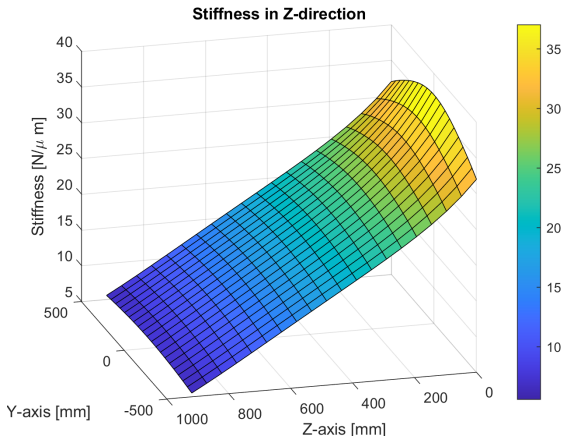


Figure 5.24: Stiffness for delta light concept for load in Z-direction at 30° head angle

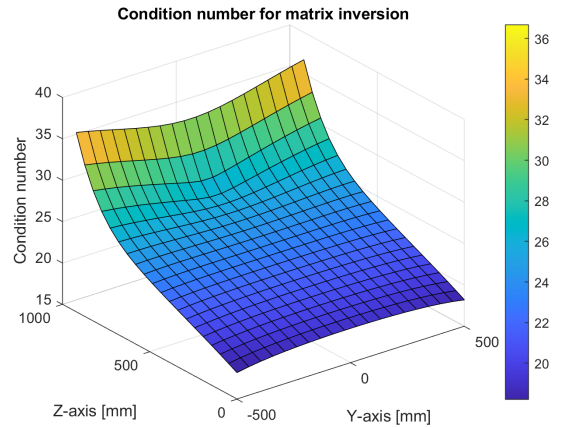


Figure 5.25: Delta light concept condition number for matrix inversion at 30° head angle

The values of the stiffness graphs without the zero values included average out to be $8.6 \text{ N}/\mu\text{m}$ in X-direction, $4.9 \text{ N}/\mu\text{m}$ in Y-direction and $18.8 \text{ N}/\mu\text{m}$ in Z-direction.

5.5.2 50 degrees

This sub chapter will show the stiffness and singularity check for the Delta Light concept at 50° positive Y-angle at the head. Figure 5.26 shows stiffness for forces in X-direction. Figures 5.27 and 5.28 show for forces in Y and Z-direction respectively. Condition number for matrix inversion for system as is can be seen in Figure 5.29.

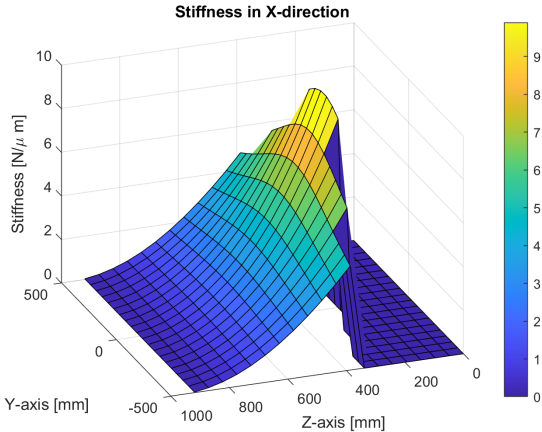


Figure 5.26: Stiffness for delta light concept for load in X-direction at 50° head angle

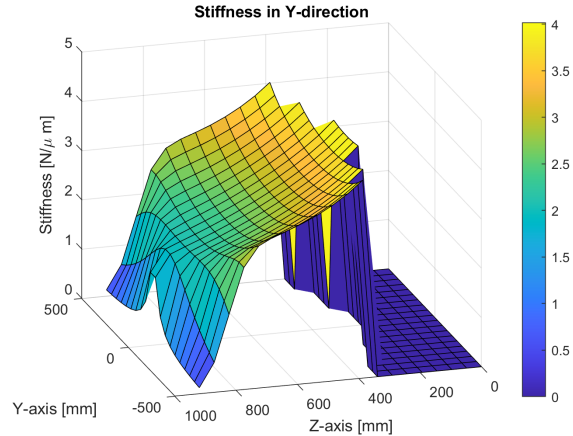


Figure 5.27: Stiffness for delta light concept for load in Y-direction at 50° head angle

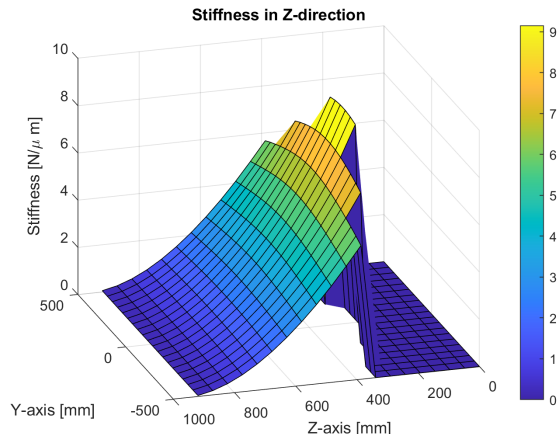


Figure 5.28: Stiffness for delta light concept for load in Z-direction at 50° head angle

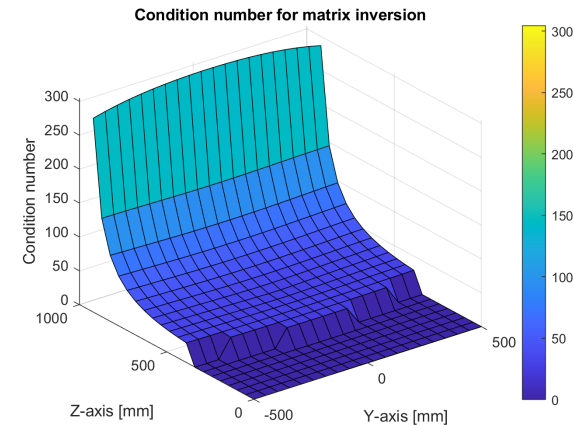


Figure 5.29: Delta light concept condition number for matrix inversion at 50° head angle

The values of the stiffness graphs without the zero values included average out to be $2.6 \text{ N}/\mu\text{m}$ in X-direction, $2.6 \text{ N}/\mu\text{m}$ in Y-direction and $2.9 \text{ N}/\mu\text{m}$ in Z-direction.

5.6 Double sled

The following two sub chapters will check the stiffness of the double sled concept for 45° and 90° rotation around Y. Checks for singularity at the position and orientation will also be done. Complete sets of stiffness and singularity graphs can be found in Appendix D.

5.6.1 45 degrees

This sub chapter will show the stiffness and singularity check for the Delta Light concept at 45° positive Y-angle at the head. Figure 5.30 shows stiffness for forces in X-direction. Figures 5.31 and 5.32 show for forces in Y and Z-direction respectively. Condition number for matrix inversion for system as is can be seen in Figure 5.33.

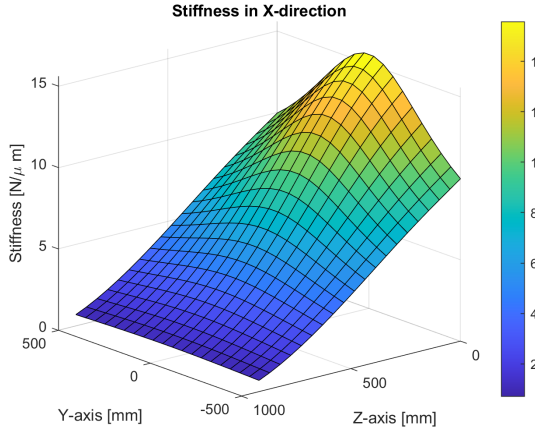


Figure 5.30: Stiffness for double sled for load in X-direction at 45° head angle

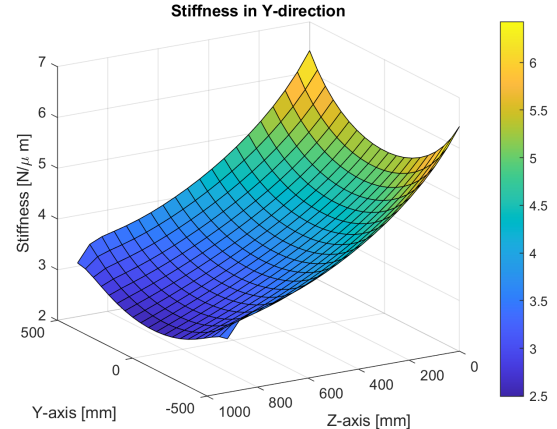


Figure 5.31: Stiffness for double sled for load in Y-direction at 45° head angle

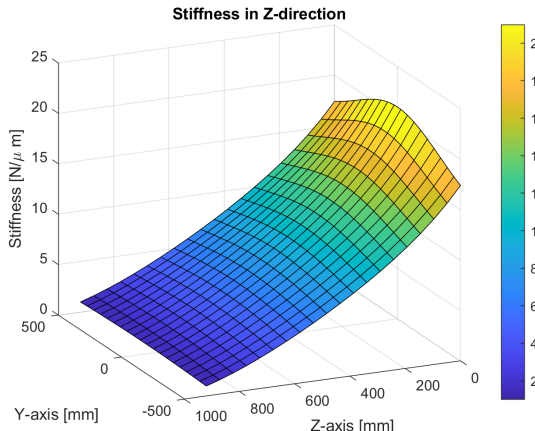


Figure 5.32: Stiffness for double sled for load in Z-direction at 45° head angle

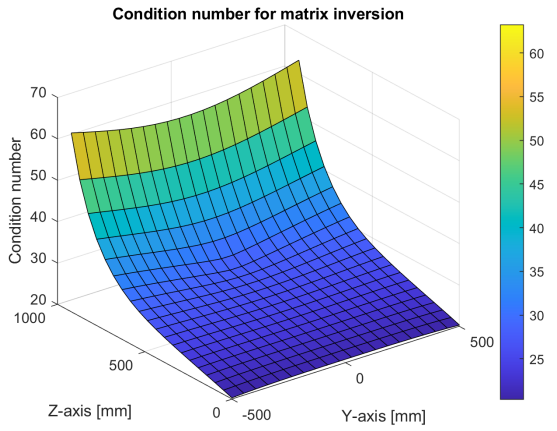


Figure 5.33: Double sled condition number for matrix inversion at 45° head angle

The values of the stiffness graphs without the zero values included average out to be $6.7 \text{ N}/\mu\text{m}$ in X-direction, $4.1 \text{ N}/\mu\text{m}$ in Y-direction and $8.8 \text{ N}/\mu\text{m}$ in Z-direction.

5.6.2 90 degrees

This sub chapter will show the stiffness and singularity check for the Delta Light concept at 90° positive Y-angle at the head. Figure 5.34 shows stiffness for forces in X-direction. Figures 5.35 and 5.36 show for forces in Y and Z-direction respectively. Condition number for matrix inversion for system as is can be seen in Figure 5.37.

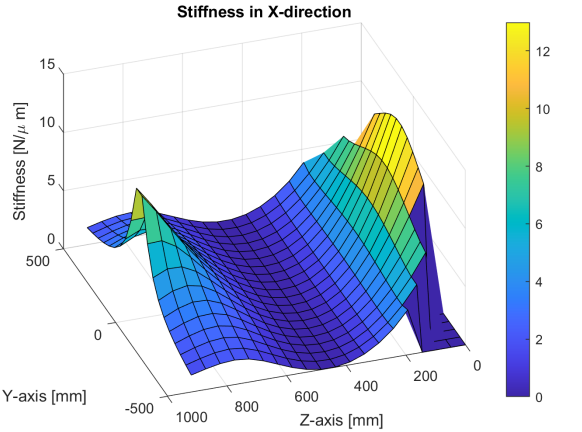


Figure 5.34: Stiffness for double sled for load in X-direction at 90° head angle

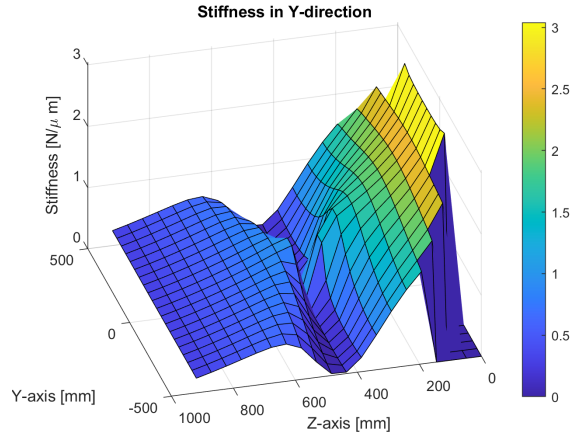


Figure 5.35: Stiffness for double sled for load in Y-direction at 90° head angle

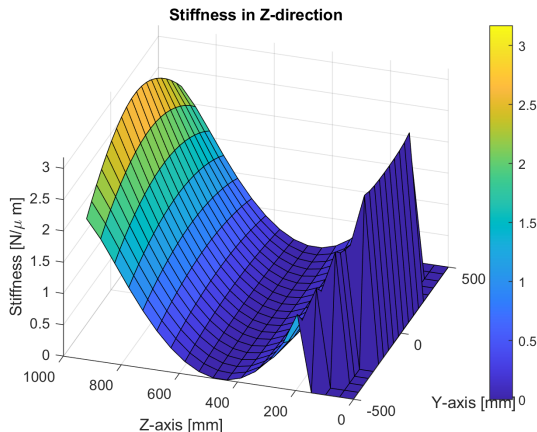


Figure 5.36: Stiffness for double sled for load in Z-direction at 90° head angle

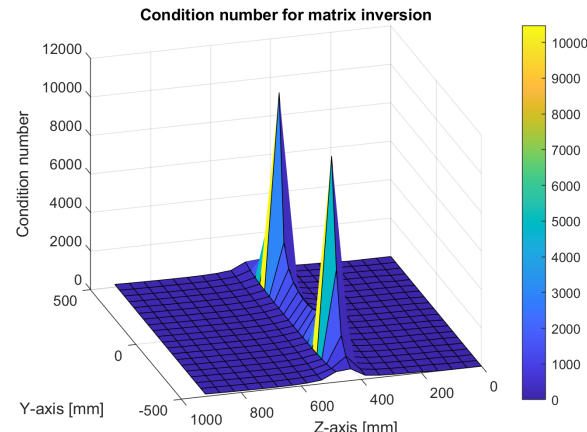


Figure 5.37: Double sled condition number for matrix inversion at 90° head angle

The values of the stiffness graphs without the zero values included average out to be $2.8 \text{ N}/\mu\text{m}$ in X-direction, $0.9 \text{ N}/\mu\text{m}$ in Y-direction and $1.0 \text{ N}/\mu\text{m}$ in Z-direction.

Chapter 6

Comparison to Original System

Reading the graphs in the previous chapter requires a lot of comparing and thinking. In this chapter a way of categorizing stiffness for future development is proposed that streamlines the process. The process involves calculating the original system's stiffness values. These values are then used in a comparison test against the concept stiffness. The comparison test value chosen is the original value multiplied with a test parameter limit, where the $limit \in [0, 1]$. The concept starts at zero rotational angle and keeps increasing angle until either a limit of 90° is reached or all the test values are larger than the current concept calculated values. The limit chosen in this chapter is 0.3. Pseudocode of the test explained above can be found below. One example of the pseudocode implemented in Matlab code script can be found in Appendix E.6.

```
testx = OldResultsx * limit;
testy = OldResultsy * limit;
testz = OldResultsz * limit;

while py < 90 AND (NewResultsx > testx OR NewResultsy > testy OR ...
    NewResultsz > testz)

    Increment angle and calculate new stiffness results of head with new ...
        rotational angle.

    if NewResultsx > testx
        plot rotational angle in x-graph
    end

    if NewResultsy > testy
        plot rotational angle in y-graph
    end

    if NewResultsz > testz
        plot rotational angle in z-graph
    end
end
```

6.1 Extending links

This chapter will present the results of the test explained in the beginning of the main chapter for the extending links concept. The results can be seen in Figures 6.1, 6.2, 6.3.

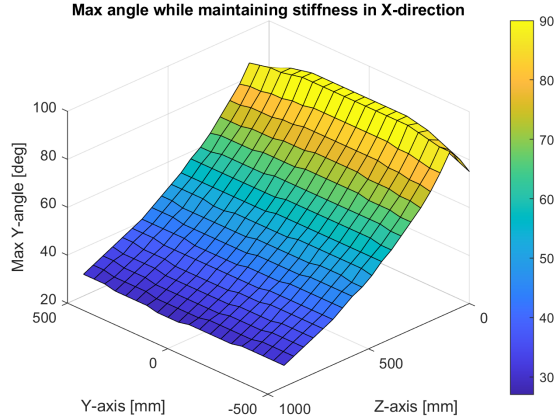


Figure 6.1: Maximum rotational angle while maintaining stiffness in X-direction

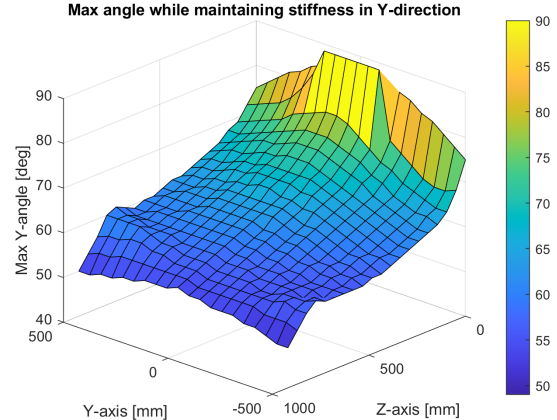


Figure 6.2: Maximum rotational angle while maintaining stiffness in Y-direction

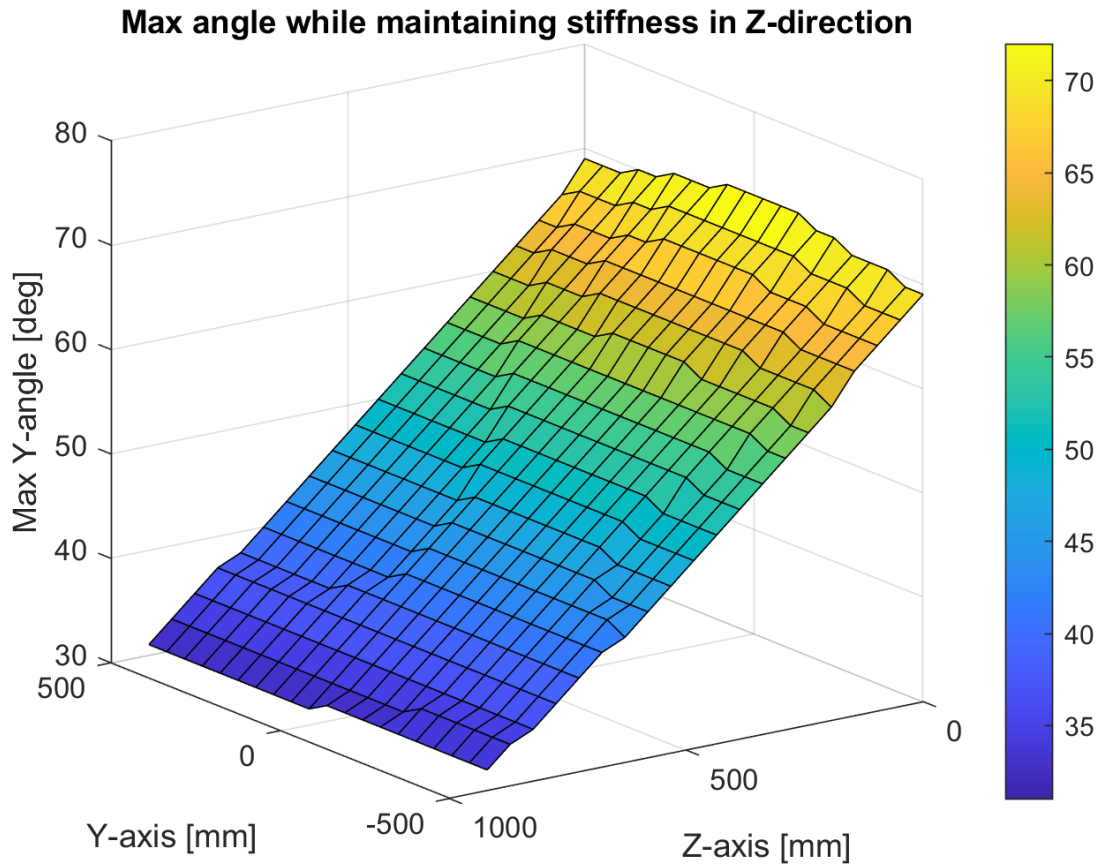


Figure 6.3: Maximum rotational angle while maintaining stiffness in Z-direction

6.2 Delta light

This chapter will present the results of the test explained in the beginning of the main chapter for the delta light concept. The results can be seen in Figures 6.1, 6.2, 6.3.

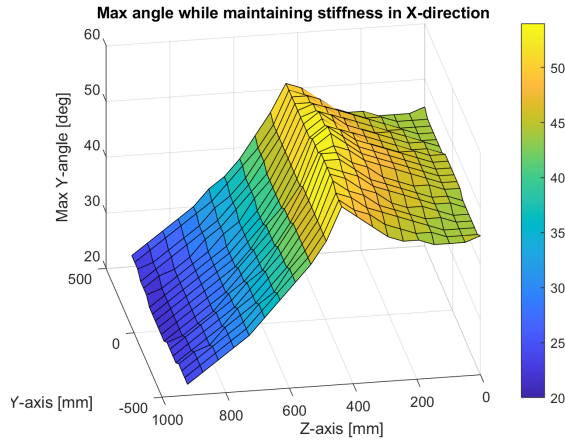


Figure 6.4: Maximum rotational angle while maintaining stiffness in X-direction

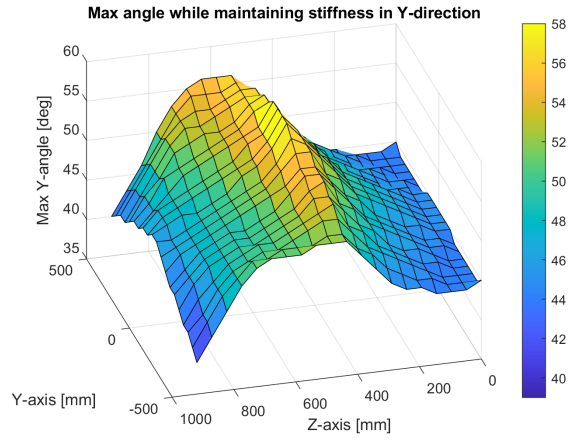


Figure 6.5: Maximum rotational angle while maintaining stiffness in Y-direction

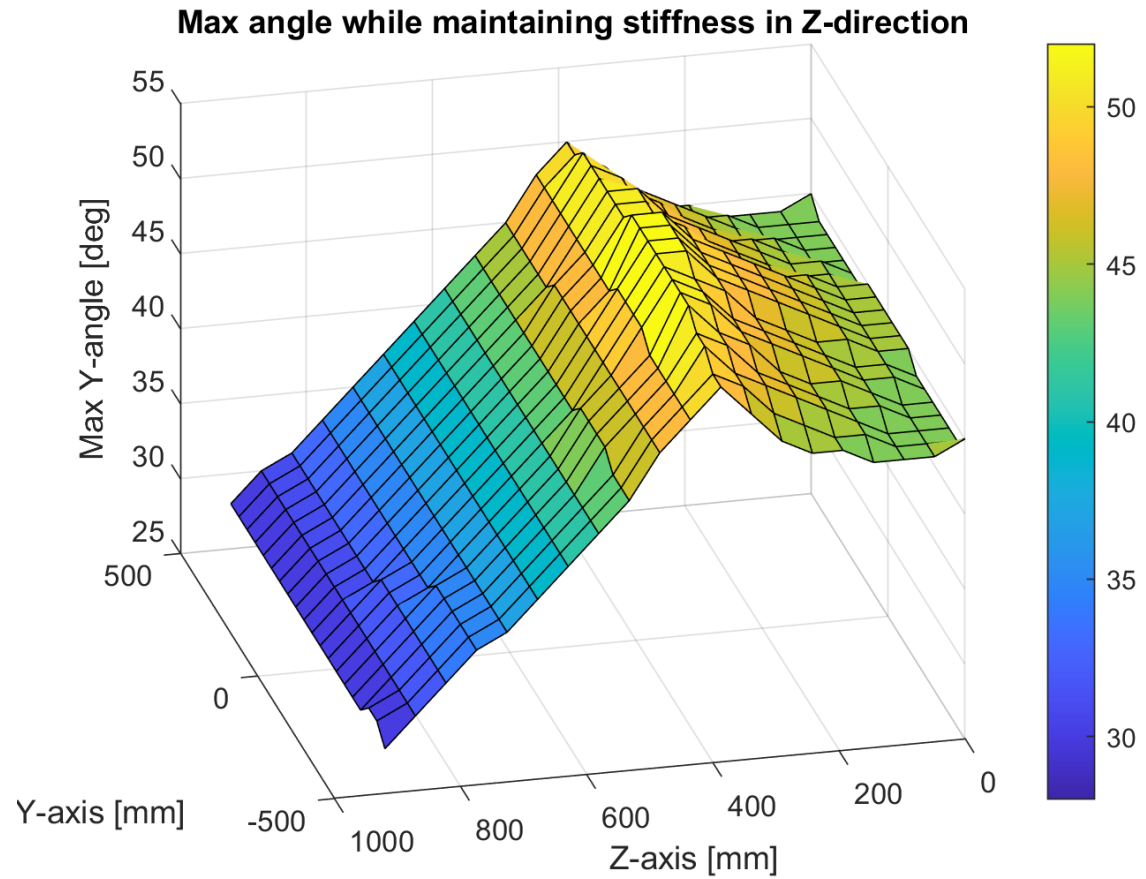


Figure 6.6: Maximum rotational angle while maintaining stiffness in Z-direction